HHS Public Access

Author manuscript

Sci Signal. Author manuscript; available in PMC 2019 April 19.

Published in final edited form as:

Sci Signal. ; 11(554): . doi:10.1126/scisignal.aar3924.

RSK2 contributes to myogenic vasoconstriction of resistance arteries by activating smooth muscle myosin and the Na^+/H^+ exchanger

Mykhaylo V. Artamonov[1], **Swapnil K. Sonkusare**[1,2], **Miranda E. Good**[2], **Ko Momotani**[1,3], **Masumi Eto**[4,5], **Brant E. Isakson**[1,2], **Thu H. Le**[1,6], **Eric L. Cope**[2], **Zygmunt S. Derewenda**[1], **Urszula Derewenda**[1], and **Avril V. Somlyo**[1,*]

[1]Department of Molecular Physiology and Biological Physics, University of Virginia, Charlottesville, VA 22908, USA

[2]Robert M. Berne Cardiovascular Research Center, University of Virginia, Charlottesville, VA 22908, USA

[3]Faculty of Pharmaceutical Sciences, Sanyo-Onoda City University, 1-1-1 Daigaku-dori, Sanyo-Onoda-shi, Yamaguchi 756-0884, Japan

[4]Department of Molecular Physiology and Biophysics, Sidney Kimmel Medical College at Thomas Jefferson University, Philadelphia, PA 19107, USA

[5]Faculty of Veterinary Medicine, Okayama University of Science, 1-13 Ikoinooka-oka, Imabari, Ehime 794-0085, Japan

[6]Department of Medicine, University of Virginia, Charlottesville, VA 22908, USA.

Abstract

Smooth muscle contraction is triggered when Ca^{2+}/calmodulin-dependent myosin light chain kinase (MLCK) phosphorylates the regulatory light chain of myosin (RLC_{20}). However, blood vessels from *Mlck*-deficient mouse embryos retain the ability to contract, suggesting the existence of additional regulatory mechanisms. We showed that the p90 ribosomal S6 kinase 2 (RSK2) also phosphorylated RLC_{20} to promote smooth muscle contractility. Active, phosphorylated RSK2 was present in mouse resistance arteries under normal basal tone, and phosphorylation of RSK2 increased with myogenic vasoconstriction or agonist stimulation. Resistance arteries from *Rsk2*-deficient mice were dilated and showed reduced myogenic tone and RLC_{20} phosphorylation. RSK2 phosphorylated Ser^{19} in RLC in vitro. In addition, RSK2 phosphorylated an activating site in the Na^+/H^+ exchanger (NHE-1), resulting in cytosolic alkalinization and an increase in intracellular Ca^{2+} that promotes vasoconstriction. NHE-1 activity increased upon myogenic

*Corresponding author. avs5u@virginia.edu.

Author contributions: A.V.S., S.K.S., M.V.A., T.H.L., Z.S.D., U.D., B.E.I., and M.E. designed the research and edited the manuscript. M.V.A., S.K.S., E.L.C., and M.E.G. performed experiments and analyzed the data. K.M. analyzed data and prepared the figures. A.V.S. wrote the manuscript.

Competing interests: The authors declare that they have no competing interests.

Data and materials availability: All data needed to evaluate the conclusions in the paper are present in the paper or the Supplementary Materials. The $Rsk2^{KO}$ mice can be obtained from W. J. Leonard (NIH).

constriction, and the increase in intracellular pH was suppressed in *Rsk2*-deficient mice. In pressured arteries, RSK2-dependent activation of NHE-1 was associated with increased intracellular Ca^{2+} transients, which would be expected to increase MLCK activity, thereby contributing to basal tone and myogenic responses. Accordingly, *Rsk2*-deficient mice had lower blood pressure than normal littermates. Thus, RSK2 mediates a procontractile signaling pathway that contributes to the regulation of basal vascular tone, myogenic vasoconstriction, and blood pressure and may be a potential therapeutic target in smooth muscle contractility disorders.

INTRODUCTION

Smooth muscle within the walls of small resistance blood vessels plays a critical role in the response to metabolic needs of the organism by contracting or relaxing to regulate blood flow and to ensure adequate oxygenation of tissues. This fundamental physiological role depends on the contractile response of smooth muscle to an increase or decrease in intraluminal pressure, known as the myogenic response (1). An increase in intraluminal pressure leads to an increase in cytosolic $[Ca^{2+}]$ and, consequently, to activation of the Ca^{2+}/calmodulin- dependent myosin light chain kinase (MLCK), phosphorylation of the myosin regulatory light chain (RLC_{20}), and initiation of cross-bridge cycling and contraction (2). An auxiliary regulatory mechanism that suppresses relaxation operates by agonist-mediated stimulation of select G protein–coupled receptors (GPCRs), which activates the RhoA-dependent kinase (ROCK), leading to phosphorylation and inhibition of the myosin light chain phosphatase (MLCP). This shift in the balance of MLCK/MLCP activities in favor of MLCK amplifies contraction at constant $[Ca^{2+}]_i$, an effect known as Ca^{2+} sensitization (3). Both pathways contribute to the myogenic response and to the contractility of resistance arteries, which are important to blood pressure homeostasis (4). However, blood vessels from smooth muscle MLCK-null embryos contract and show increased RLC_{20} phosphorylation in response to both agonists and Ca^{2+} (5), and smooth muscle contracts in response to MLCP inhibitors in the absence of Ca^{2+} (6). These effects show that additional MLCK-independent signaling or phosphorylation mechanisms of physiological importance operate in smooth muscle. In addition, several kinases other than MLCK have been proposed to play auxiliary roles in smooth muscle regulation. They include the zipper-interacting kinase (DAPK3) (7), integrin-linked kinase (ILK) (8), IκBK (inhibitor κB kinase 2) (9), and Pim kinase (10). A newly developed dual Pim/DAPK3 inhibitor reduces caudal artery contractility and decreases blood pressure in spontaneously hypertensive mice (10). These kinases phosphorylate RLC_{20}, leading to smooth muscle contraction, but their specific physiological roles in the myogenic response have not been studied. Another Ser/Thr kinase reported to phosphorylate RLC_{20} in vitro is the p90 ribosomal S6 kinase (RSK) (11). We have shown that in isolated blood vessels, RSK-specific inhibitors suppress both Ca^{2+}- and agonist-induced contractile force and reduce phosphor ylation of RLC_{20} (12). Furthermore, agonist stimulation leads to activation of extracellular signal–regulated kinase 1/2 (ERK1/2) and phosphoinositide- dependent kinase 1 (PDK1), both of which are required to phosphorylate and fully activate RSK (12). Although ERK1/2 and PDK1 play physiologically relevant roles in the activation of smooth muscle contraction and cell proliferation (13, 14), RSKs have not been implicated as their downstream effectors in smooth muscle. Because of the importance of vascular resistance in the determination of

blood pressure, a full understanding of the pathways that regulate basal vascular tone and smooth muscle contractility is essential to develop new approaches to treat diseases such as hypertension and asthma, which involve smooth muscle dysfunction and—in many cases—do not respond well to current therapies.

There are four isoforms of RSK (RSK1 to RSK4), and all share an unusual molecular architecture with two enzymatic kinase domains in tandem: a regulatory C-terminal kinase domain (CTKD) and an N-terminal kinase domain (NTKD), connected by a linker sequence with several functionally important phosphorylation sites. The activation mechanism is complex (Fig. 1A). Of the four isoforms, RSK1 and RSK2 are expressed in a more ubiquitous manner, and RSK2 is the more plausible candidate in smooth muscle (12). For RSK2, activation is initiated by ERK1/2 docking to a sequence motif downstream of CTKD and phosphorylating Thr^{577} in the CTKD activation loop, as well as Thr^{365} and Ser^{369} within the linker. The activated CTKD carries out cis-phosphorylation of Ser^{386} within the so-called hydrophobic motif of the linker region, to create a docking site for PDK1 that phosphorylates the NTKD on Ser^{227} in the activation loop, resulting in a fully active enzyme (15). To follow RSK2 phosphorylation as a measure of its activity, we developed a method to pressurize arcades of mouse mesenteric arteries to have sufficient material to follow RSK2 phosphorylation status (Fig. 1B).

Increased RSK activity has been reported in aortic cells from spontaneously hypertensive compared to normal rats (16). RSK has also been identified in cultured aortic smooth muscle cells as a putative kinase for the Na^+/H^+ exchanger isoform-1 (NHE-1), which controls intracellular pH and cell volume (17, 18). Activating phosphorylation of NHE-1 on Ser^{703} is increased in cultured smooth muscle cells from spontaneously hypertensive rats (SHR) and is linked to hypertension in humans (19, 20). Activation of NHE-1 and cytosolic alkalinization are associated with vasoconstriction [reviewed in (20)], but the mechanism underlying the vasoconstriction is unknown. Furthermore, it is not known whether or how RSK2 signaling through NHE-1 might contribute to the myogenic response, vascular resist ance, and blood pressure control.

There is considerable interest in the physiological functions of RSK2. Mutations in its gene, *Rps6ka3*, are associated with a rare, debilitating neurological developmental genetic disorder called Coffin-Lowry syndrome (CLS) (21), which is recapitulated in mice lacking the gene ($Rps6ka3^{-/-}$) (22). However, no studies of the cardiovascular system in these animals (referred to as $Rsk2^{KO}$) or patients have been described. We now report that $Rsk2^{KO}$ mice had dilated resistance arteries, lower myogenic tone, reduced vascular myosin RLC_{20} phosphorylation, and decreased basal blood pressure. In normal mice, we detected low levels of activating phosphorylation of RSK2, RLC_{20}, and NHE-1, consistent with the involvement of this signaling pathway in basal blood pressure maintenance, and the phosphorylation of these proteins was increased during the myogenic contraction of mesenteric resistance arteries. As with RLC_{20}, activation of NHE-1 in mesenteric arteries depended on RSK2 activity. Moreover, RSK2 activation of NHE-1 increased intracellular pH and led to an increase in intracellular Ca^{2+} and augmented MLCK-dependent myosin activation. Our findings provide new insights into mechanisms for the modulation of blood flow in

resistance arteries and blood pressure regulation, opening new avenues for future drug discovery.

RESULTS

Rsk2^{KO} mice have normal vasculature and normal expression of proteins involved in contractility

As previously reported (22), aged-matched male and female *Rsk2*^{KO} mice (fig. S1A) were significantly smaller than normal animals (WT = 30 ± 1.8*g*, $n = 6$ and *Rsk2*^{KO} = 19.3 ± 0.9*g*, $n = 6$, $P < 0.05$), but were nevertheless fertile and had normal life spans and healthy coats. The animals have supernumerary teeth typical of the CLS phenotype, which is characterized by craniofacial and dental abnormalities (22, 23). Histology of second-, third-, and fourth-order mesenteric arteries from *Rsk2*^{KO} mice showed no obvious differences in structure or in the number of smooth muscle layers in the vessel wall compared to normal animals (fig. S1B and table S1). Acetylcholine- induced dilation of mesenteric arteries isolated from *Rsk2*^{KO} mice, a measure of endothelial viability, was identical to that of arteries from normal animals (fig. S1C). Levels of myosin, actin, MLCK, ROCK, and MYPT1, as well as those of the guanosine triphosphate (GTP) exchange factors p63RhoGEF, LARG, and GEFH1, were similar in *Rsk2*^{KO} and wild-type (WT) mice; similarly, the abundance of the G proteins $G\alpha_{q11}$ and $G\alpha_{12}$, both of which are involved in Ca^{2+} sensitization, was also similar in *Rsk2*^{KO} and WT mice (fig. S2).

Small mesenteric arteries from *Rsk2*^{KO} mice are dilated with reduced myogenic constriction compared to vessels from normal animals

First, we assessed whether the *Rsk2*^{KO} genotype affected the myogenic tone of small resistance arteries, as determined by pressure myography. We measured changes in diameter in isolated, small (140 to 180 μm diameter), third- and fourth-order mesenteric arteries upon pressurization from 20 to 100 mmHg (Fig. 1C). Arteries from *Rsk2*^{KO} mice constricted to a significantly lesser extent with each increased pressure step compared to vessels from normal littermates (Fig. 1D). Constriction in response to increases in added K^+ were similar between *Rsk2*^{KO} and WT arteries, indicative of a normal depolarization-induced response (fig. S1D). Phenylephrine-induced responses were similar in both types of vessels, and median effective concentration (EC_{50}) values for phenylephrine- induced contractions were not significantly different (Fig. 1E). However, the concentration response curve was statistically significantly shifted vertically for *Rsk2*^{KO} vessels, reflecting reduced initial tone.

Intraluminal pressure activates RSK2 in mesenteric arteries by 30 s, leading to increased phosphorylation of RLC_{20}

Next, we followed the time course of phosphorylation of both RSK2 and RLC_{20} in mesenteric arteries in response to increase in intraluminal pressure from 0 to 80 mmHg using our pressurized mesenteric artery arcades. Specifically, we monitored the phosphorylation of RLC_{20} on Ser^{19} and of RSK2 on Thr^{577} (mediated by ERK) and Ser^{227} (mediated by PDK1) (Fig. 1, F and G), using antibodies that we demonstrated to be specific (fig. S3, A to C). Phosphorylation of RSK2 on Ser^{227} increased significantly by 30 s, the

first time point measured following the pressure step, whereas phosphorylation of RSK2 on Thr^{577} increased by 90 s (Fig. 1G). In the resting state, we observed detectable, basal phosphorylation of both regulatory sites on RSK2, consistent with the notion that RSK2 signaling contributes to basal vessel tone (Fig. 1F). Phosphorylation of RLC_{20} on Ser^{19} was significantly higher in normal vessels than in *Rsk2*^{KO} vessels under basal conditions (Fig. 1G). After pressurization, RLC_{20} phosphorylation increased significantly within 30 s in both normal and *Rsk2*^{KO} arteries but to a significantly lesser extent in the *Rsk2*^{KO} arteries (Fig. 1G). Phosphorylation of RLC_{20} is most likely the outcome of the combined and concurrent activities of MLCK, MLCP, and RSK2. Nevertheless, the onset of RSK2 activation was sufficiently fast enough to contribute to the pressure-induced myogenic response and accounts for ~25% of total RLC_{20} phosphorylation.

RSK2 inhibitors relax myogenic tone and decrease RSK2 phosphorylation

To confirm the contribution of RSK2 to contraction of normal blood vessels, we used the selective pan-RSK inhibitor LJH685 (24). Increasing concentrations of LJH685 significantly relaxed mesenteric artery myogenic constriction induced by 80 mmHg pressure (Fig. 2A). Preincubation of smooth muscle cells with the RSK2 inhibitor LJH685 and the ERK inhibitor U0126 significantly suppressed serum-induced phosphorylation of Ser^{227} in RSK2 (Fig. 2B). Inhibition by U1026 is consistent with the canonical scheme of RSK activation, in which RSK is downstream of the mitogen- activated protein kinase (MAPK) cascade (Fig. 1A). These observations further implicate RSK signaling as a critical contributor to the contractile state of vascular smooth muscle.

Agonists induce RSK2 and RLC_{20} phosphorylation in mouse mesenteric arteries

We next investigated whether agonist- mediated stimulation of mesenteric arteries also activated RSK2 signaling. We monitored the time course of phosphorylation of RSK2 and of RLC_{20} in response to endothelin-1 (ET-1), angiotensin II (AngII), the thromboxane analog U46619, and phenylephrine in nonpressurized artery arcades. Within 30 s, phenylephrine stimulation led to a significant increase in RSK2 phosphorylation on both regulatory sites (Ser^{227} and Thr^{577}), whereas the other agonists took 90 s to reach a significant increase at these sites (Fig. 3). MYPT1, the regulatory subunit of MLCP, was phosphorylated on Thr^{853} (a site that is a substrate for ROCK) within 30 to 90 s after stimulation of mesenteric arteries with ET-1, AngII, U46619, or phenylephrine, with ET-1 having the largest effect. These agonists activate the RhoA/ROCK signaling pathway, leading to Ca^{2+} sensitization in other blood vessels, but it is not known whether RSK2 regulates this pathway. RLC_{20} Ser^{19} phosphorylation peaked at 30 s upon U46619 and phenylephrine stimulation and at 90 s upon ET-1 stimulation. Agonist-induced RLC_{20} phosphorylation levels are expected to reflect increased cytosolic Ca^{2+}–driven MLCK activity and RhoA/ROCK- mediated inhibition of MLCP as shown in other arteries (3, 25). On the basis of the time course of activation of RSK2 phosphorylation by the four agonists and by the suppression of phenylephrine-induced contraction (Fig. 1E), our data suggest that RSK2 activity also contributes to agonist-induced RLC_{20} phosphorylation in mesenteric arteries, with phenylephrine being the most potent agonist. Last, phosphorylation was detectable on all RSK2 and MYPT1 sites under resting conditions, consistent with a contribution of RSK2 and RhoA/ROCK activity to basal resting tone in these vessels.

RSK2 phosphorylates RLC_{20} but does not activate MLCP activity

Using purified, recombinant RSK2 and purified RLC_{20}, we confirmed that when fully phosphorylated and activated by ERK2 and PDK1, RSK2 directly phosphorylated RLC_{20} on Ser^{19} (Fig. 4A). Purified MLCK served as a positive control. As we have reported that recombinant, activated RSK2 phosphorylated the phosphatase MYPT1 on Ser^{668} (12), we determined whether this phosphorylation event changed MLCP activity by measuring the ability of MLCP thiophosphorylated by RSK2 or ROCK2 to dephosphorylate phospho-RLC_{20}. MLCP activity was not inhibited by thiophosphorylation of MYPT1 by RSK2 but, as expected, was decreased by ROCK2, which phosphorylates MYPT1 on both Thr^{696} and Thr^{853} (Fig. 4B) (26). In mesenteric arteries, the phosphorylation of MYPT1 on ROCK site, Thr^{853}, was similar in normal and $Rsk2^{KO}$-derived vessels (Fig. 4C) at all three time points after pressurization. Thus, we conclude that RSK2 does not directly modulate MLCP activity in vitro and does not alter the ROCK-mediated phosphorylation of Thr^{853} in MYPT1 during pressurization of arteries.

A fraction of RSK2, like MLCK, is associated with actin filaments

Because RSK2 directly phosphorylated RLC_{20} Ser^{19}, mimicking the role of MLCK, we questioned whether RSK2 also bound to actin filaments in a manner similar to MLCK. We found that antibodies for RSK2 immunoprecipitated actin from normal mouse aortic smooth muscle cells (Fig. 4D) and mouse aorta (fig. S4). RSK2 did not coimmunoprecipitate myosin [smooth muscle myosin heavy chain 11 (MYH11) and RLC_{20}] (fig. S4). Neither RSK2 nor actin was detected in control samples from $Rsk2^{KO}$ smooth muscle or from beads in the absence of RSK2 antibodies (Fig. 4D). After highspeed centrifugation to separate the cytoskeletal (200,000*g* pellet) and cytosolic (supernatant) fractions in lysates from resting and pressurized mesenteric arteries, RSK2, MLCK, and actin were found in both pellet and the supernatant (Fig. 4E). Although the supernatant contained G actin monomers and small actin fragments, RSK2 in the supernatant was largely free rather than actin bound, because the amount detected did not change significantly with latrunculin B and cytochalasin or jasplakinolide treatment to favor depolymerization or polymerization of the actin cytoskeleton, respectively (Fig. 4F). We conclude that in a manner similar to MLCK, a fraction of RSK2 is localized to the actin cytoskeleton, which may enable phosphorylation of RLC_{20}.

Intraluminal pressure stimulates RSK2-dependent phosphorylation of NHE-1 to induce cytosolic alkalinization and an associated increase in $[Ca^{2+}]_i$ in mesenteric arteries

Because NHE-1 is a phosphorylation target for RSK2, we determined the impact of the loss of RSK2 on NHE-1 phosphorylation in smooth muscle. We found that under resting conditions, the phosphorylation of NHE-1 on Ser^{703} was greater in normal than in $Rsk2^{KO}$ mesenteric arteries (Fig. 5A). The RSK inhibitors LJH685 and LJI308 both significantly reduced the phosphorylation of Ser^{703} (Fig. 5B.). Upon pressurization of normal mesenteric arteries to 80 mmHg, the phosphorylation of Ser^{703} increased significantly within 30 s (Fig. 5C). RSK2 antibody immunoprecipitated NHE-1 from mesenteric artery tissue homogenates (Fig. 5D). Together, these data indicate that Ser^{703} in NHE-1 is phosphorylated by RSK2, that RSK2 is associated with NHE-1, and that the time course of NHE-1 phosphorylation in

response to intraluminal pressure is fast enough for this phosphorylation event to contribute to myogenic vasoconstriction. We then asked whether RSK2 regulated NHE-1 activity in blood vessels. We monitored intracellular pH with the ratiometric fluorescent pH indicator BCECF-AM in arteries pressurized to 60 mmHg in the presence of Na^+-containing physiological salt solution (Fig. 6A), lacking CO_2/HCO_3^- to eliminate activity of the Na^+/HCO_3^- exchanger. After pressurization, which led to alkalinization, NHE-1 activity was inhibited by removal of Na^+ from the perfusate, which resulted in a decrease in intracellular pH. Re-addition of Na^+ led to a statistically significant increase in pH in WT arteries, an increase that was statistically significantly suppressed in *Rsk2*^{KO} arteries. The rate and magnitude of recovery upon the addition of Na^+ served as a direct measure of NHE-1 activity. The magnitude of the recovery was statistically significantly greater in WT than in *Rsk2*^{KO} arteries, and the response was faster. Thus, RSK2 contributes to the regulation of NHE-1 activity in pressurized resistance arteries.

Increased RSK2 and NHE-1 activities have been reported in hypertensive rodents and humans, and we hypothesized that this was due to an increase in intracellular Ca^{2+} resulting in arterial constriction. Therefore, we set out to determine whether stimulation of NHE-1 correlated with an increase in $[Ca^{2+}]_i$. Because NHE-1 is stimulated by both low pH and phosphorylation, we first applied an acid pulse to stimulate NHE-1 activity (27). Monitoring of $[Ca^2]_i$ with Fluo-4 in acid load–stimulated cells revealed a significant increase in $[Ca^{2+}]_i$ in normal mouse aortic smooth muscle cells, but not in *Rsk2*^{KO} cells (Fig. 6B and fig. S5), and that this increase was blocked by the NHE-1 inhibitor cariporide (28).

To investigate the correlation between intraluminal pressure, NHE-1 activity, and Ca^{2+}-transient events, we imaged individual smooth muscle cells within an intact pressurized mesenteric artery loaded with Fluo-4 (Fig. 6C and movie S1). Increasing the intraluminal pressure from 20 to 60 mmHg resulted in more Ca^{2+} transient events. Conversely, the number of Ca^{2+} transient events was reduced at 60 mmHg by the NHE-1 inhibitor cariporide (Fig. 6C). Arteries were also treated with ryanodine to deplete ryanodine-sensitive Ca^{2+} stores but not inositol trisphosphate (IP_3)–mediated Ca^{2+} stores (29). Ryanodine reduced the number of Ca^{2+} transients (Fig. 6, C and D). At the higher pressure, cariporide significantly reduced the number of transients irrespective of the presence or absence of ryanodine (Fig. 6, C and D). Thus, RSK2 activation of NHE-1 activity is correlated with an increase in intracellular Ca^{2+} that is partially released from ryanodine-sensitive Ca^{2+} stores.

Rsk2^{KO} mice have decreased basal blood pressure and normal cardiac output compared to WT animals

Last, we investigated the possibility that blood pressure may be affected in *Rsk2*^{KO} mice due to altered vascular smooth muscle regulation. As measured by the tail cuff method during the day, the resting systolic blood pressure in both male and female *Rsk2*^{KO} mice was significantly lower compared to WT littermates (Fig. 7A). This finding was confirmed using radiotelemetry in male mice, which also showed normal circadian rhythm in *Rsk2*^{KO} mice (Fig. 7A). Heart rates (table S2), electrocardiogram intervals (table S2), or heart/body weight ratios (Fig. 7B) did not differ between the normal and *Rsk2*^{KO} mice, although *Rsk2*^{KO} mice are smaller than WT mice, as reflected in the reduced heart wall thicknesses (Fig. 7B). To

assess whether the lower basal blood pressure was correlated with cardiac abnormalities in *Rsk2*^{KO} mice, magnetic resonance imaging (MRI) imaging and histology were used to evaluate heart morphology and function (Fig. 7, C and D, and table S2). Although heart chamber mass and end-diastolic and systolic volumes were all lower in the *Rsk2*^{KO} mice, as expected from their smaller size, cardiac function as indicated by ejection fraction (Fig. 7B) and cardiac output (table S2) did not differ. Histological sections taken at mid-level of the ventricles showed no abnormalities (Fig. 7D). Thus, a dilated myocardium and/or defective cardiac function are unlikely to account for the decrease in blood pressure in the *Rsk2*^{KO} mice.

DISCUSSION

Here, we present evidence that RSK2 signaling in smooth muscle in resistance arteries contributes to an increase in vascular resistance and blood pressure (Fig. 7E). We identified two downstream targets of RSK2 that mediate the enhanced vascular tone: RLC_{20} and NHE-1. Specifically, we found that small mesenteric resistance vessels from *Rsk2*^{KO} mice exhibited impaired myogenic responsiveness compared to vessels from normal mice. This did not appear to reflect differences in $[Ca^{2+}]_i$, because $[Ca^{2+}]_i$ was not significantly different in the unstimulated normal and *Rsk2*^{KO} cultured aortic cells (Fig. 6B). The decrease in RLC_{20} phosphorylation in the *Rsk2*^{KO} arteries compared to normal arteries could reflect the loss of the ability of RSK2 to phosphorylate RLC_{20} independently of an increase in Ca^{2+}. In normal murine vessels, the activating phosphorylation of RSK2 and RLC_{20} was statistically significantly increased by 30 s after pressurization. Although the time course of RLC_{20} phosphorylation in *Rsk2*^{KO} vessels was similar, the maximum level was reduced by ~30%, both in the absence of pressure and after pressurization to 80 mmHg. Myogenic tone was also suppressed in *Rsk2*^{KO} by ~25% compared to normal arteries (Fig. 1D). Likewise, an RSK-specific inhibitor suppressed myogenic contraction by ~25%. Together, these experiments suggest that the maximal contribution of RSK2 to myogenic force can reach ~25%. Furthermore, suppression of force by the RSK inhibitor demonstrated that the effect correlated specifically with RSK activity and is unlikely to be due to secondary changes in smooth muscle due to the altered genotype in *Rsk2*^{KO} mice. Apart from a role in myogenic vasoconstriction, phosphorylation of RSK2, NHE-1, and RLC_{20} was consistently and reproducibly detected under basal conditions, suggesting that RSK2 signaling is a component of constitutive activity contributing to resting vessel tone.

Stimulation with ET-1, AngII, phenylephrine, and the thromboxane analog U46619, which increase $[Ca^{2+}]_i$ and activate Ca^{2+}- sensitized force, all statistically significantly increased activating phosphorylation of RSK2 by 90 s, with phenylephrine having the greatest effect and being readily detected by 30 s. Phenylephrine contractile responses were suppressed by ~25% in arteries from *Rsk2*^{KO} mice (Fig. 1E), giving an estimate for the contribution of RSK2 to vasoconstriction, at least for this agonist in mesenteric arteries. We have previously reported that the ROCK inhibitor Y27632 inhibits U46619-induced contraction in pulmonary arteries by about 60%, and subsequent addition of an RSK inhibitor reduces it further to about 10% above baseline (12). Thus, the RSK contribution to contraction is not through modulating MLCP activity, as directly confirmed in the present study (Fig. 4B) and can be separated from the Ca^{2+} sensitization component. Ca^{2+} sensitization monitored by

phosphorylation at the ROCK site, MYPT1 Thr^{853}, increased in response to all agonists, with ET-1 being the most potent. Studies in other blood vessels show that the contribution of Ca^{2+} sensitization to contractile responses varies with different agonists, as does the magnitude of the Ca^{2+} transient (3). Our data suggest that in mouse mesenteric arteries, ET-1 signals through the Rho/ROCK pathway to inhibit MLCP to a greater extent than phenylephrine, which is more effective in activating RSK2 than ET-1. RLC_{20} phosphorylation was several fold above baseline in the presence of all agonists by 5 min except for angiotensin. The initial rise reflects the early onset of the agonist-induced Ca^{2+} transient that, in other vessels, precedes RhoA/Rho kinase–induced activation of Ca^{2+} sensitization. The later onset of Ca^{2+} sensitization maintains force and RLC_{20} phosphorylation, although $[Ca^{2+}]_i$ has fallen (30). For example, $[Ca^{2+}]_i$ has been reported to rise within 150 ms, whereas RhoA-GTP increases with a 10-s lag after release of phenylephrine from caged phenylephrine in portal vein (30). We have not resolved whether RSK2 activity contributes to early or late tension maintenance upon phenylephrine stimulation. However, we can conclude that all four agonists studied can activate RSK2 in mouse mesenteric arteries, with phenylephrine being the most potent, and that these agonists also activate RhoA/ROCK-mediated Ca^{2+} sensitization of force to different extents. An intriguing question focuses on the importance of these multiple signaling pathways and their agonist selectivity in driving vasoconstriction, and whether it is to provide redundancy for this critical function or to provide a more phasic or tonic type contraction to meet physiological demand or whether the different pathways and agonists uniquely activate additional pathways with different functions, such as smooth muscle proliferation.

Upstream signaling from agonists through GPCRs to RSK2 includes ERK-induced phosphorylation of RSK2, which is critical for its activation (Fig. 1A). ERK is activated by phenylephrine, AngII, other agonists, growth factors, and integrins in various smooth muscle types. Multiple downstream targets of ERK have been implicated, including calponin, caldesmon, CPI17, and ILK, but their role in contractility is controversial. We suggest that RSK2 is a tenable downstream substrate of ERK and that it mediates ERK-associated contractility. Signaling upstream of ERK leads to c-Src–dependent transactivation of epidermal growth factor receptor, resulting in activation of Ras-, Raf-, MAPK kinase (MEK)–, and ERK-mediated cell growth and vascular remodeling by agonist-coupled GPCRs and mitogens (31). NHE-1 has also been implicated in proliferation of smooth muscle such as in pulmonary hypertension. Thus, RSK2 may also play a role in vascular wall remodeling such as occurs in hypertension.

Resting blood pressure was statistically significantly lower in both male and female $Rsk2^{KO}$ mice than in their normal littermates, in agreement with the lower resting tone and RLC_{20} phosphorylation in the mice mesenteric vessels. Heart size/body weight and function evaluated by MRI were normal in the $Rsk2^{KO}$ mice, suggesting that the decreased blood pressure was not due to decreased cardiac output. However, direct measures are needed to firmly establish that a decrease in vascular resistance is the root cause of the lower blood pressure. The regulation of normal and increased blood pressure is a complex phenomenon. The kidney is generally considered to play a key role. However, there is considerable evidence that changes in vascular tone alone are sufficient to cause hypotension or hypertension (32–34). Our study has not determined a causal effect of vascular tone on

blood pressure, but rather a correlation of the lower blood pressure, RLC_{20} phosphorylation, and dilated resistance vessels with the *Rsk2*^{KO} genotype, and does not preclude the role of RSK2 in kidney function. Mice with conditional knockout of RSK2 in smooth muscle, which would need to be generated and investigated in future studies, would not exclude renal vascular effects on blood pressure but would address possible nonspecific or compensatory effects.

The myogenic response is essential for blood flow autoregulation. We found that both RSK2 and NHE-1 contribute to myogenic contraction. NHE-1 in cardiac myocytes is also proposed to be mechanically sensitive, responding to muscle stretch or osmotic cell shrinkage with increased $[Na^+]_i$ and $[Ca^{2+}]_i$ (35, 36) and to be ERK1/2 dependent (37). We propose that ERK1/2 activation of NHE-1 is mediated by RSK2 possibly through mechanosensitive integrins that activate ERK1/2 (38) and are involved in the myogenic response (39, 40).

Experiments using *Rsk2*^{KO} arteries showed that RSK2 is a critical upstream activator of NHE-1–induced alkalinization associated with increased $[Ca^{2+}]_i$ and myogenic vasoconstriction. Resting pH in rodent mesenteric arteries is governed largely by a balance between acid extrusion by NHE-1 and the Na^+- bicarbonate$^-$ transporter (41). The relationship between smooth muscle pH and contraction is complex and varies in different kinds of blood vessels (42). Changes in pH_i are tightly linked to $Ca^{2+}{}_i$ signaling and changes in artery tone (43). Acidosis generally inhibits the Na^+/Ca^{2+} exchanger (44), the sarcoplasmic reticulum (SR) and plasmalemmal Ca^{2+} adenosine triphosphatases (ATPases) (45, 46), L-type Ca^{2+} channels (47), and the SR ryanodine-sensitive Ca^{2+} release channels (42), resulting in muscle relaxation (28). IP_3- and Ca^{2+}- induced Ca^{2+} release are also increased with alkalinization (42). The increase in Ca^{2+} associated with the RSK2/NHE-1–mediated alkalinization is expected to augment MLCK activity, RLC_{20} phosphorylation, and myogenic vasoconstriction. These observations provide an explanation for the correlation of increased RSK2 and NHE-1 activities found in vascular smooth muscle when stimulated by AngII and the increased Na^+/H^+ exchange activity associated with hypertension. In addition, these observations may explain the correlation between platelet aggregation, $[Ca^{2+}]_i$, pH_i, and blood pressure as observed in treated and untreated hypertensive patients (48). Enhanced NHE-1 and RSK2 activity under pathological conditions and metabolic challenges would be expected to increase NHE-1–induced alkalinization and artery dysfunction, whereas under normal conditions the Na-bicarbonate exchanger would tend to buffer the large changes in pH that we observed with the myogenic response (43).

Ca^{2+} influx and/or release from the SR through IP_3 receptor or ryanodine receptors, distributed over the continuous SR network in smooth muscle cells (49, 50), result in various distinctive cytosolic Ca^{2+} transients (51, 52). We observed Ca^{2+} transients in pressurized arteries, with or without treatment with ryanodine (which depletes Ca^{2+} stores), and both were suppressed by cariporide. These findings show that SR ryanodine-sensitive Ca^{2+} stores regulated by NHE-1 activity are a source of the Ca^{2+} transients induced in myogenic vasoconstriction. IP_3-initiated Ca^{2+} waves that propagate across the entire muscle cell from an initial release site (53) become inactivated at high $[Ca^{2+}]$, accounting for the transient Ca^{2+} wave (movie S1) (54). Regardless of whether Ca^{2+} waves are sourced from Ca^{2+} influx, IP_3- or ryanodine-sensitive stores, or all sources, our main finding is that inhibition of

NHE-1 suppressed Ca^{2+} transients in arteries and that NHE-1 activity is RSK2 dependent. Future studies will focus on the molecular mechanisms responsible for the $[Na^+]$- and $[H^+]$-induced regulation of Ca^{2+} handling and contractility in smooth muscle of small resistance arteries, both under normal and pathological conditions.

We found RSK2 and MLCK in the supernatant of artery homogenates, suggesting that they partition between the soluble and filament- enriched fractions. MLCK has been proposed to tether to actin through its N terminus and then to reach across the 40-nm gap to interact with myosin heads (55). However, it is difficult to explain the ability of 1 to 4 μM concentrations of MLCK, when tethered to actin, to phosphorylate the majority of the ~100 μM myosin heads, and the same concern would apply to actin-bound RSK2. Further, RSK2 phosphorylates various cytosolic substrates, so it reasonable to expect that some portion remains fully solubilized in the cytosol and available to membrane-associated NHE-1. The C terminus of NHE-1 also acts as a membrane anchor for actin filaments through binding to the ERM family protein, ezrin, and is thus able to regulate cell shape and migration (56). Last, RhoA/ROCK activity, which induces Ca^{2+} sensitization with myogenic arterial contraction (57), may regulate NHE-1 activity (58). NHE-1 C-terminal modifications by other kinases and the binding of regulatory proteins, such as calmodulin, also alter the affinity of the NHE-1 transmembrane binding domain for H^+_i (59). Thus, multiple regulatory processes may further modify NHE-1 activity. Their potential contributions to essential hypertension with dysfunctional Ca^{2+} regulation in smooth muscle remain to be investigated. In conclusion, RSK2 provides a new procontractile signaling pathway that contributes to the regulation of basal vascular tone, myogenic vasoconstriction, and blood pressure.

MATERIALS AND METHODS

Rsk2^{KO} mice

Rsk2^{KO} mice were a gift from W. J. Leonard [National Institutes of Health (NIH)] (60); they were generated as reported previously (22) and characterized (fig. S1, A to D). RSK1 and RSK3 protein expression levels in *Rsk2*^{KO} mice have been reported to be similar to those in normal mice (22). All animal studies were performed under protocols that comply with the *Guide for the Care and Use of Laboratory Animals* and were approved by the Animal Care and Use Committee at our institution.

Pressure myography

Freshly isolated third- or fourth-order mesenteric arteries (<180 μm) were placed into Hepes-Krebs solution (118.4 mM NaCl, 4.7 mM KCl, 1.2 mM $MgSO_4$, 4 mM $NaHCO_3$, 1.2 mM KH_2PO_4, 2 mM $CaCl_2$, 10 mM Hepes, and 6 mM glucose) and then mounted in a pressure arteriograph (Danish MyoTechnology or a custom made device), as previously described (61, 62). The vessels were pressurized to 20 mmHg and then to 60 or 80 mmHg at 37°C and equilibrated for 30 min, brought back to 20 mmHg, and then exposed to incremental increases in pressure to 100 mmHg. Vessels were used only if they displayed robust endothelial cell viability, which was assessed at the end of an agonist-induced constriction using 10 μM acetylcholine (fig. S1C) (61) or the calcium activated intermediate

(IK) or small conductance (SK) channel agonist NS309 to induce relaxation of a myogenic constriction (63). Luminal diameters were measured in response to changes in intraluminal pressure or to cumulative concentrations of phenylephrine or inhibitors applied to the circulating bath. Responses to cumulative concentrations of high K^+ were achieved by increasing the K^+ concentration from 5.9 to 62 mM by substituting equal volumes of Hepes-Krebs solution with depolarizing Hepes-Krebs solution (143.3 mM KCl, 1.2 mM $CaCl_2$*$2H_2O$, 1.2 mM $MgCl_2$*$6H_2O$, 11.6 mM Hepes, and 11.5 mM dextrose) while keeping Ca and Mg concentrations constant. Maximum inner diameter was measured after washing with a Ca^{2+}-free Krebs-Hepes solution supplemented with 1 mM EGTA and 10 μM sodium nitroprusside. Quantification of vessel diameter was performed using the DMT software MyoView. Basal tone and vasoconstriction values were calculated as follows: [maximum diameter − active diameter/maximum diameter] × 100. Acetylcholine and phenylephrine data are expressed as the percentage of the maximum inner diameter.

Preparation of pressurized mesenteric artery cascades

Arcades of mesentery vessels amenable to pressurization to mimic the myography were developed to have a sufficient amount of vessel material to carry out biochemical experiments (Fig. 1B). Whole mesenteric artery arcades (arteries of second to fourth order) were dissected from mice, and all open ends were closed with suture, incubated for 1 hour at 37°C in Hepes-Krebs buffer, cannulated, and pressurized to 80 mmHg using a sphygmomanometer (Riester Big-Ben Round, Germany). Before and immediately after a pressure step or agonist stimulation, arcades were frozen at 30 s, 90 s, and 5 min, respectively, and analyzed for phosphorylation of MYPT1 at Thr^{668} and Thr^{853}, RLC_{20} at Ser^{19}, RSK at Thr^{577}/Ser^{227}, PDK1 at Ser^{241}, and NHE-1 Ser^{703}. Tissues were snap frozen in liquid nitrogen and transferred to a vial with 10% cold trichloroacetic acid/acetone to preserve the phosphorylation state as described previously (25). Agonists were AngII (1 μM) or endothelin 1 (10 nM), phenylephrine (1 μM), and TXA2 receptor mimetic U46619 (1 μM).

pH measurements

Freshly isolated third-fourth-order mesenteric arteries from WT and *Rsk2*^{KO} mice were incubated with 2 μM BCECF-AM (Thermo Fisher Scientific, B1170) at 37°C for 20 min and extensively washed with Hepes-Krebs solution, mounted in a pressure arteriography chamber (The Instrumentation and Model Facility, University of Vermont, Burlington, VT, USA). Andor Revolution WD (with Borealis) spinning disc confocal imaging system was used to record intracellular pH. pH measurements were made by determining the ratio of emission intensity recorded using a 525/36-nm bandpass filter when the dye is excited at ~488-nm solid-state laser (pH dependent) compared to the emission intensity when the dye is excited at its isosbestic point of ~435 nm (non–pH dependent) with a light- emitting diode light source (pE-4000, CoolLED Ltd., Andover, UK), as described previously (64). After loading, vessels were equilibrated at 37°C for 15 min at 20 mmHg and superfused (flow rate, ~3 ml/min) with Hepes-Krebs (pH 7.3) with the lumen filled with Krebs-Hepes solution. pH images were recorded over 300 ms period taken every minute. Three samples were recorded at 20 mmHg, and five samples were recorded at 60 mmHg. Upon Na^+ removal by replacing Hepes-Krebs buffer with Hepes-Krebs Na^+-free buffer (NaCl was

substituted with equimolar concentration of *N*-methyl-D-glucamine; Sigma-Aldrich, catalog number: M2004; pH 7.3). Seven samples were recorded, and upon reintroduction of Na^+ with Krebs-Hepes solution, 10 samples were recorded. At the end of each experiment, an in situ calibration curve was established. Arteries were treated with nigericin (Sigma-Aldrich, catalog number: N7143) and exposed to high K^+ depolarizing Hepes-Krebs solution of varying pH (6.3, 6.6, 6.9, 7.2, and 7.5) to equilibrate internal and external pH (65). Background signal was collected in a mesenteric artery not loaded with BCECF-AM at 525 nm after excitation at 435 and 488 nM. pH was calculated as the ratio of 435/488 nm signal with background signal subtracted for each wavelength and pH interpreted from the calibration curve.

Ca^{2+} measurements

Ca^{2+} signals in cultured smooth muscle cells grown from abdominal aortae from 2-month-old normal and *Rsk2*^{KO} mice and in third-order branches of mesenteric arteries. These cells were used to determine the role of RSK2 in regulating NHE-1 activity stimulated by a brief acid load because they allowed continuous Ca^{2+} monitoring during the brief transient change in pH. Cells were imaged using an Andor Revolution WD (with Borealis) spinning disc confocal imaging system (Andor Technology, Belfast, UK), composed of an upright Nikon microscope with a 40× water-dipping objective (numerical aperture, 0.8) and an electron-multiplying charge-coupled device camera (63). For Ca^{2+} imaging of smooth muscle cells, cells were plated on glass bottom culture dishes (MatTek Corporation) and maintained in AmnioMAX medium plus supplement. Cells were incubated with Fluo-4 AM (Thermo Fisher Scientific) for 1 hour and washed with Hepes-Krebs solution, and Ca^{2+} fluorescence was recorded as follows: (i) Hepes-Krebs, (ii) Hepes-Krebs–buffered 80 mM Na acetate (27), (iii) Hepes-Krebs, (iv) Hepes-Krebs–buffered 80 mM Na acetate in the presence of cariporide, (v) Hepes-Krebs, and (vi) ionomycin. Equimolar Na acetate replaced NaCl in the control solution, and $CaCl_2$ was increased to 1.37 mM to keep [Ca^{2+}] constant. Ca^{2+} concentrations were measured in a 1.7-μm^2 region encompassing multiple confluent cells. Images were recorded from 12 to 22 cells in a field, with 999 frames taken for each field, and the mean and SEM were calculated for each condition. Fluorescence at saturating Ca^{2+} was measured after ionomycin treatment and used to calculate [Ca^{2+}] (66). Mean Fluo-4 fluorescent intensities were as follows: WT control, NaAC, and ionomycin treatment = 536, 559, and 665, respectively, and *Rsk2*^{KO} = 544, 530, and 637, respectively. For Ca^{2+} imaging of arteries, third-fourth-order branches of mesenteric arteries (~100 μm internal diameter at 80 mmHg) were isolated into Hepes-Krebs, loaded with Fluo-4 AM (10 μM) for 1 hour, washed for 30 min with Hepes-Krebs, cannulated, and incubated without or with 10 μM ryanodine to inhibit ryanodine receptors, and fluorescent events were recorded. Images were recorded at 60 frames s^{-1} under the following conditions: basal pressure at 20 mmHg, 60 mmHg, and 60 mmHg plus cariporide (30 μM). Fluo-4–bound Ca^{2+} was detected by exciting at 488 nm with a solid-state laser and collecting emitted fluorescence using a 527.5- to 49-nm bandpass filter.

Measurement of blood pressure

Systolic blood pressure was measured in conscious male and female mice (15 WT and 9 *Rsk2*^{KO}, ages 5 to 15 months) by tail cuff using an MC4000MSP system (Hatteras

Instruments Inc.). Animals were conditioned by placing them on the apparatus platform for 15 min/day on two consecutive weeks, and “sham” measurements were taken. On the next two consecutive weeks, mice were placed on the platform daily, and at least 10 readings were taken. Conditioning and all blood pressure readings were performed at the same location, by the same operator, at the same time of day under quiet, low-light conditions. Two groups of 10- to 15-month-old and 5- to 7-monthold $Rsk2^{KO}$ mice and their WT littermates were used. There was no statistically significant difference in blood pressure values between the two groups, so the data were pooled. Radiotelemetric blood pressure monitoring was measured in three WT and seven $Rsk2^{KO}$ conscious male mice of the same age under unrestrained conditions. Continuous blood pressure measurements were performed using Dataquest A.R.T. 20 software (Data Sciences International, St. Paul, MN), as described previously (67). Mice were allowed to recover for 7 days after surgery to regain their normal circadian rhythms before blood pressure measurements were initiated. Baseline systolic, diastolic, and mean arterial pressures and heart rate were recorded continuously over 7 days (at 1-min intervals) after the recovery period. The values over 7 × 24-hour periods were averaged to obtain the baseline day- or nighttime blood pressures.

Cardiac MRI and histology

These experiments were performed as described previously (68). A 30-mm-diameter cylindrical birdcage radiofrequency coil (Bruker) with an active length of 70 mm was used, and heart rate, respiration, and temperature were monitored during imaging using a fiber-optic, MR-compatible system (Small Animal Imaging Inc., Stony Brook, NY). MRI was performed on a 7-T ClinScan system (Bruker, Ettlingen, Germany) equipped with actively shielded gradients with a full strength of 650 mT/m and a slew rate of 6666 mT m^{-1} ms^{-1}. Baseline left ventricular structure and function were assessed (68). Six short-axis slices were acquired from base to apex, with slice thickness equal to 1 mm, in-plane spatial resolution of 0.2 × 0.2 mm^2, and temporal resolution of 8 to 12 ms. Baseline ejection fraction, end-diastolic volume (EDV), end-systolic volume (ESV), myocardial mass, wall thickness, and wall thickening were measured from the cine images using the freely available software Segment version 2.0 R5292 (http://segment.heiberg.se). EDV and ESV were then indexed to body mass. Mass-to-volume ratio was calculated as the ratio of myocardial mass to EDV.

Assay for RSK2 phosphorylation of RLC_{20}

Recombinant RSK2 was expressed, purified, and activated according to our established protocol (69), with an additional purification step using Strep-Tactin resin before final size exclusion. RLC_{20} (100 μM) purified from turkey gizzard was incubated with either activated RSK2 (0.12 μM) or MLCK (0.28 μM) purified from turkey gizzard, serving as a positive control, for 10 min at 30°C in buffer containing 25 mM Mops-NaOH (pH 7.0), 10 mM $MgCl_2$, 1 mM EGTA, 5% glycerol, 1 μM microcystin-LR (MCLR), 1 mM adenosine triphosphate (ATP), 4 mM Pefabloc, and 0.5 mM tris (2-carboxyethyl) phosphine hydrochloride (TCEP). Sample buffer was added to the reaction mix, and samples were heated to 100°C for 5 min and subjected to electrophoresis and Western blotting. RLC_{20} phosphorylation was expressed as the ratio of RLC Ser^{19} phosphorylation to total RLC protein.

Phosphatase assay

The assays for MLCP were conducted as described previously (69). Briefly, thiophosphorylation of recombinant MLCP complex (0.6 μg: FLAG/MAT/Venus-MYPT1 + 3xHA-PP1δ) was carried out for 2 hours at 30°C with RSK2 (12 mU/μl; BioVision) or ROCK2 (27 mU/μl; SignalChem) in the presence of 0.1 mM ATPγS and terminated by adding 2 μM staurosporine. Aliquots of the thiophosphorylated MLCP were mixed with 2 μM P-RLC_{20} (3–20) peptide as substrate. After 60-min incubation, at room temperature, phosphate released from the substrate was assayed using the Malachite green method (BioMol). The MLCP activity without ATPγS was set as 100%. RSK2 activity was confirmed by phospho-dot blotting using RLC_{20} as substrate.

WT and *Rsk2^{KO}* primary aortic smooth muscle cells

Cultured smooth muscle cells were prepared from abdominal aortas from 2-month-old WT and *Rsk2^{KO}* mice, cleaned of adventitia, cut into 1 mm^2 pieces, and left undisturbed for 10 days in culture medium. Cells grown in serum-free medium were stimulated with serum in the presence and absence of LJH685 (10 μM), the PDK1 inhibitor GSK2334470 (10 μM), and the ERK1/2 inhibitor U0126 (10 μM) added 4 hours before serum stimulation for 5 min.

RSK2 actin association assays

Mesenteric artery arcades and aortae from WT mice and WT and *Rsk2^{KO}* primary aortic smooth muscle cells were used for ultracentrifugation and immunoprecipitation experiments. For immunoprecipitation assays, WT and *RSK2^{KO}* mouse aortic smooth muscle cells were starved for 72 hours and lysed in radioimmunoprecipitation assay (RIPA) buffer supplemented with protease inhibitor cocktail (PIC) (Sigma-Aldrich) and phosphatase arrest I (G-Biosciences). After equilibrating at 37°C for 1 hour, the TXA2R agonist U46619 (1 μM) was added to abdominal aorta samples for 90 s before lysis. Lysates were centrifuged for 10 min at 4°C, 20,000*g*, and supernatant was applied to Protein G Sepharose 4 Fast Flow beads (GE Healthcare) preincubated with or without RSK2 monoclonal antibody (Santa Cruz Biotechnology) and incubated at 4°C for 2 hours. After centrifugation, beads were washed (four times) with RIPA buffer and prepared for gel electrophoresis. For ultracentrifugation experiments, mouse aortic smooth muscle cells (~90% confluency) or mesenteric artery arcades pressurized at 80 mmHg for 90 s were pretreated with or without jasplakinolide (200 nM) or latrunculin B (10 μM) plus cytochalasin D (10 μM) for 30 min. Preparations were lysed in low-salt buffer containing 50 mM NaCl, 50 mM tris, 5 mM $MgCl_2$, 1 mM EGTA (pH 7.3), 1% PIC, and 1% phosphatase arrest I. Debris was precleared at 20,000*g*, and supernatant was centrifuged at 200,000*g* for 4 hours at 4°C in a Beckman Optima TLX ultracentrifuge. Pellet and supernatant were prepared for gel electrophoresis.

Immunoprecipitation assays

Lysates of mesenteric artery arcades were centrifuged for 10 min at 4°C, 20,000*g*, and supernatant was applied to Protein G Sepharose 4 Fast Flow beads (GE Healthcare) preincubated with or without RSK2 monoclonal antibody (Santa Cruz Biotechnology) and incubated at 4°C for 2 hours. After centrifugation, beads were washed (four times) with RIPA buffer and prepared for gel electrophoresis.

Western blotting

Proteins were transferred to polyvinylidene difluoride membranes and blocked with Odyssey blocking buffer, probed with primary antibodies in blocking buffer, and detected and quantified on the Odyssey system (LI-COR). The following antibodies were used: mouse monoclonal and rabbit polyclonal anti-actin (1:5000 WB; Sigma-Aldrich), mouse monoclonal anti-RLC_{20} (1:1000 WB; Sigma-Aldrich), rabbit polyclonal anti-RLC_{20} phospho-Ser^{19} (1:200 WB; Cell Signaling), mouse monoclonal anti-MYPT1 (1:1000 WB; BD Biosciences), rabbit polyclonal anti-MYPT1 Thr^{853} (1:200 WB; Cell Signaling), rabbit polyclonal anti-MYPT1 Thr^{696} (1:500 WB; Cell Signaling), rabbit polyclonal anti-MYPT1 Thr^{668} (1:500 WB; Cell Signaling), rabbit polyclonal antibodies anti-RSK2 phospho-Ser^{227}/phospho-Thr^{577} and mouse monoclonal anti-RSK2 (1:500 WB; 1:50 IP; Santa Cruz Biotechnology Inc.), phospho-Ser^{227}/phospho-Thr^{577} blocking peptides SC12445 and SC3744664 (Santa Cruz Biotechnology Inc.), sheep polyclonal anti–NHE-1 phospho-Ser^{703} (1:500 WB; MRC-PPU Reagents), mouse monoclonal (1:200 WB; Millipore) and rabbit polyclonal anti–NHE-1 (1:100 WB; LSBio), mouse monoclonal anti-MLCK (1:500 WB; Sigma-Aldrich), mouse monoclonal anti- caveolin2 (1:200 WB; Cell Signaling), rabbit polyclonal anti-histone3 (1:200 WB; Cell Signaling), rabbit polyclonal anti-MYH11 (1:500 WB), mouse monoclonal anti-tubulin (1:5000 WB; Millipore), GAPDH (1:5000 WB; Millipore), anti-LARG (1:100 WB; Santa Cruz Biotechnology Inc.), p63RhoGEF (GEFT) (1:200 WB; Proteintech Group Inc.), anti-GEFH1 (1:200 WB; Cell Signaling), rabbit polyclonal anti-$G\alpha_{q/11}$ (1:500 WB; Santa Cruz Biotechnology Inc.), rabbit polyclonal anti-$G\alpha_{12}$ (1:300 WB; Santa Cruz Biotechnology Inc.), and anti-ROCK2 goat polyclonal (1:300 WB; Santa Cruz Biotechnology Inc.). Primary antibodies were detected with either goat anti-rabbit or anti-mouse Alexa Fluor 680 (1:10,000, Invitrogen), donkey anti-sheep Alexa Fluor 680 (1:10,000, Invitrogen), or a goat anti-rabbit and anti-mouse IRDye800 (1:10,000, Rockland Immunochemicals)–conjugated secondary antibody.

Data analysis

Data are presented as means ± SE. Statistical significance was determined using the two-tailed Student's *t* test (Microsoft Excel) and one-way ANOVA (GraphPad Prism) and Tukey's post hoc test. The level of statistical significance was set at $P < 0.05$.

Supplementary Material

Refer to Web version on PubMed Central for supplementary material.

Acknowledgments:

We thank W. J. Leonard (NIH) for providing the $Rsk2^{KO}$ mouse strain. We are also grateful to J. Roy (Molecular Imaging Core Facility) for MRI analysis and excellent advice, as well as to B. French and D. A. Cornejo for the interpretation of the MRI studies. **Funding:** A.V.S., Z.S.D., and U.D. were supported by NIH R01 GM086457; B.E.I. was supported by NIH R01 HL088554; T.H.L. was supported by NIH R01 DK R01 DK113632; M.E.G. was supported by NIH training grants HL007284 and HL131399; and S.K.S. was supported by HL121484 and HL138496.

REFERENCES AND NOTES

1. Bayliss WM, On the local reactions of the arterial wall to changes of internal pressure. J. Physiol 28, 220–231 (1902). [PubMed: 16992618]
2. Somlyo AP, Somlyo AV, Signal transduction and regulation in smooth muscle. Nature 372, 231–236 (1994). [PubMed: 7969467]
3. Somlyo AP, Somlyo AV, Ca^{2+} sensitivity of smooth muscle and nonmuscle myosin II: Modulated by G proteins, kinases, and myosin phosphatase. Physiol. Rev 83, 1325–1358 (2003). [PubMed: 14506307]
4. Cole WC, Welsh DG, Role of myosin light chain kinase and myosin light chain phosphatase in the resistance arterial myogenic response to intravascular pressure. Arch. Biochem. Biophys 510, 160–173 (2011). [PubMed: 21392499]
5. Somlyo AV, Wang H, Choudhury N, Khromov AS, Majesky M, Owens GK, Somlyo AP, Myosin light chain kinase knockout. J. Muscle Res. Cell Motil 25, 241–242 (2004). [PubMed: 15467390]
6. Gong MC, Cohen P, Kitazawa T, Ikebe M, Masuo M, Somlyo AP, Somlyo AV, Myosin light chain phosphatase activities and the effects of phosphatase inhibitors in tonic and phasic smooth muscle. J. Biol. Chem 267, 14662–14668 (1992). [PubMed: 1321813]
7. MacDonald JA, Borman MA, Murányi A, Somlyo AV, Hartshorne DJ, Haystead TAJ, Identification of the endogenous smooth muscle myosin phosphatase-associated kinase. Proc. Natl. Acad. Sci. U.S.A 98, 2419–2424 (2001). [PubMed: 11226254]
8. Wilson DP, Sutherland C, Borman MA, Deng JT, Macdonald JA, Walsh MP, Integrin-linked kinase is responsible for Ca^{2+}-independent myosin diphosphorylation and contraction of vascular smooth muscle. Biochem. J 392, 641–648 (2005). [PubMed: 16201970]
9. Ying Z, do Carmo JM, Xiang L, da Silva AA, Chen M, Ryan MJ, Ostrowski M, Rajagopalan S, Hall JE, Inhibitor κB kinase 2 is a myosin light chain kinase in vascular smooth muscle. Circ. Res 113, 562–570 (2013). [PubMed: 23817200]
10. Carlson DA, Singer MR, Sutherland C, Redondo C, Alexander LT, Hughes PF, Knapp S, Gurley SB, Sparks MA, MacDonald JA, Haystead TAJ, Targeting Pim kinases and DAPK3 to control hypertension. Cell Chem. Biol 25, 1195–1207.e32 (2018). [PubMed: 30033129]
11. Suizu F, Ueda K, Iwasaki T, Murata-Hori M, Hosoya H, Activation of actin-activated MgATPase activity of myosin II by phosphorylation with MAPK-activated protein kinase-1b (RSK-2). J. Biochem 128, 435–440 (2000). [PubMed: 10965042]
12. Artamonov M, Momotani K, Utepbergenov D, Franke A, Khromov A, Derewenda ZS, Somlyo AV, The p90 ribosomal S6 kinase (RSK) is a mediator of smooth muscle contractility. PLOS ONE 8, e58703 (2013). [PubMed: 23516539]
13. Dessy C, Kim I, Sougnez CL, Laporte R, Morgan KG, A role for MAP kinase in differentiated smooth muscle contraction evoked by α-adrenoceptor stimulation. Am. J. Physiol 275, C1081–C1086 (1998). [PubMed: 9755061]
14. Kuemmerle JF, IGF-I elicits growth of human intestinal smooth muscle cells by activation of PI3K, PDK-1, and p70S6 kinase. Am. J. Physiol. Gastrointest. Liver Physiol 284, G411–G422 (2003). [PubMed: 12444011]
15. Pearce LR, Komander D, Alessi DR, The nuts and bolts of AGC protein kinases. Nat. Rev. Mol. Cell Biol 11, 9–22 (2010). [PubMed: 20027184]
16. Siczkowski M, Davies JE, Ng LL, Na^+-H^+ exchanger isoform 1 phosphorylation in normal Wistar-Kyoto and spontaneously hypertensive rats. Circ. Res 76, 825–831 (1995). [PubMed: 7728999]
17. Takahashi E, Abe J, Berk BC, Angiotensin II stimulates p90rsk in vascular smooth muscle cells. A potential Na^+-H^+ exchanger kinase. Circ. Res 81, 268–273 (1997). [PubMed: 9242188]
18. Phan VN, Kusuhara M, Lucchesi PA, Berk BC, A 90kD Na^+/H^+ exchanger kinase has increased activity in spontaneously hypertensive rat vascular smooth muscle cells. Hypertension 29, 1265–1272 (1997). [PubMed: 9180627]
19. Takahashi E, Abe J.-i., Gallis B, Aebersold R, Spring DJ, Krebs EG, Berk BC, $p90^{RSK}$ is a serum-stimulated Na^+/H^+ exchanger isoform-1 kinase. Regulatory phosphorylation of serine 703 of Na^+/H^+ exchanger isoform-1. J. Biol. Chem 274, 20206–20214 (1999). [PubMed: 10400637]

20. Touyz RM, Schiffrin EL, Signal transduction mechanisms mediating the physiological and pathophysiological actions of angiotensin II in vascular smooth muscle cells. Pharmacol. Rev 52, 639–672 (2000). [PubMed: 11121512]
21. Trivier E, De Cesare D, Jacquot S, Pannetier S, Zackai E, Young I, Mandel J-L, Sassone-Corsi P, Hanauer A, Mutations in the kinase Rsk-2 associated with Coffin-Lowry syndrome. Nature 384, 567–570 (1996). [PubMed: 8955270]
22. Dufresne SD, Bjørbæk C, El-Haschimi K, Zhao Y, Aschenbach WG, Moller DE, Goodyear LJ, Altered extracellular signal-regulated kinase signaling and glycogen metabolism in skeletal muscle from p90 ribosomal S6 kinase 2 knockout mice. Mol. Cell. Biol 21, 81–87 (2001). [PubMed: 11113183]
23. Laugel-Haushalter V, Paschaki M, Marangoni P, Pilgram C, Langer A, Kuntz T, Demassue J, Morkmued S, Choquet P, Constantinesco A, Bornert F, Schmittbuhl M, Pannetier S, Viriot L, Hanauer A, Dollé P, Bloch-Zupan A, RSK2 is a modulator of craniofacial development. PLOS ONE 9, e84343 (2014). [PubMed: 24416220]
24. Aronchik I, Appleton BA, Basham SE, Crawford K, Del Rosario M, Doyle LV, Estacio WF, Lan J, Lindvall MK, Luu CA, Ornelas E, Venetsanakos E, Shafer CM, Jefferson AB, Novel potent and selective inhibitors of p90 ribosomal S6 kinase reveal the heterogeneity of RSK function in MAPK-driven cancers. Mol. Cancer Res 12, 803–812 (2014). [PubMed: 24554780]
25. Neppl RL, Lubomirov LT, Momotani K, Pfitzer G, Eto M, Somlyo AV, Thromboxane A_2-induced bi-directional regulation of cerebral arterial tone. J. Biol. Chem 284, 6348–6360 (2009). [PubMed: 19095646]
26. Kawano Y, Fukata Y, Oshiro N, Amano M, Nakamura T, Ito M, Matsumura F, Inagaki M, Kaibuchi K, Phosphorylation of myosin-binding subunit (Mbs) of myosin phosphatase by Rho-kinase in vivo. J. Cell Biol 147, 1023–1038 (1999). [PubMed: 10579722]
27. Swietach P, Spitzer KW, Vaughan-Jones RD, Na^+ ions as spatial intracellular messengers for co-ordinating Ca^{2+} signals during pH heterogeneity in cardiomyocytes. Cardiovasc. Res 105, 171–181 (2015). [PubMed: 25514933]
28. Garciarena CD, Youm JB, Swietach P, Vaughan-Jones RD, H^+-activated Na^+ influx in the ventricular myocyte couples Ca^{2+}-signalling to intracellular pH. J. Mol. Cell. Cardiol 61, 51–59 (2013). [PubMed: 23602948]
29. Nelson MT, Cheng H, Rubart M, Santana LF, Bonev AD, Knot HJ, Lederer WJ, Relaxation of arterial smooth muscle by calcium sparks. Science 270, 633–637 (1995). [PubMed: 7570021]
30. Artamonov MV, Momotani K, Stevenson A, Trentham DR, Derewenda U, Derewenda ZS, Read PW, Gutkind JS, Somlyo AV, Agonist-induced Ca2+ sensitization in smooth muscle: Redundancy of Rho guanine nucleotide exchange factors (RhoGEFs) and response kinetics, a caged compound study. J. Biol. Chem 288, 34030–34040 (2013). [PubMed: 24106280]
31. Mehta PK, Griendling KK, Angiotensin II cell signaling: Physiological and pathological effects in the cardiovascular system. Am. J. Physiol. Cell Physiol 292, C82–C97 (2007). [PubMed: 16870827]
32. Mendelsohn ME, In hypertension, the kidney is not always the heart of the matter. J. Clin. Invest 115, 840–844 (2005). [PubMed: 15841174]
33. Crowley SD, Gurley SB, Oliverio MI, Pazmino AK, Griffiths R, Flannery PJ, Spurney RF, Kim H-S, Smithies O, Le TH, Coffman TM, Distinct roles for the kidney and systemic tissues in blood pressure regulation by the renin-angiotensin system. J. Clin. Invest 115, 1092–1099 (2005). [PubMed: 15841186]
34. Wirth A, Wang S, Takefuji M, Tang C, Althoff TF, Schweda F, Wettschureck N, Offermanns S, Age-dependent blood pressure elevation is due to increased vascular smooth muscle tone mediated by G-protein signalling. Cardiovasc. Res 109, 131–140 (2016). [PubMed: 26531127]
35. Cingolani HE, Alvarez BV, Ennis IL, Camilión de Hurtado MC, Stretch-induced alkalinization of feline papillary muscle: An autocrine-paracrine system. Circ. Res 83, 775–780 (1998). [PubMed: 9776724]
36. Whalley DW, Hemsworth PD, Rasmussen HH, Sodium-hydrogen exchange in guinea-pig ventricular muscle during exposure to hyperosmolar solutions. J. Physiol 444, 193–212 (1991). [PubMed: 1668347]

37. Vaughan-Jones RD, Spitzer KW, Swietach P, Intracellular pH regulation in heart. J. Mol. Cell. Cardiol 46, 318–331 (2009). [PubMed: 19041875]
38. Juliano RL, Signal transduction by cell adhesion receptors and the cytoskeleton: Functions of integrins, cadherins, selectins, and immunoglobulin-superfamily members. Annu. Rev. Pharmacol. Toxicol 42, 283–323 (2002). [PubMed: 11807174]
39. Martinez-Lemus LA, Crow T, Davis MJ, Meininger GA, $\alpha_V\beta_3$- and $\alpha_5\beta_1$-integrin blockade inhibits myogenic constriction of skeletal muscle resistance arterioles. Am. J. Physiol. Heart Circ. Physiol 289, H322–H329 (2005). [PubMed: 15722407]
40. Colinas O, Moreno-Domínguez A, Zhu H-L, Walsh EJ, Pérez-Garcia MT, Walsh MP, Cole WC, α_5-Integrin-mediated cellular signaling contributes to the myogenic response of cerebral resistance arteries. Biochem. Pharmacol 97, 281–291 (2015). [PubMed: 26278977]
41. Boedtkjer E, Damkier HH, Aalkjaer C, NHE1 knockout reduces blood pressure and arterial media/lumen ratio with no effect on resting pH_i in the vascular wall. J. Physiol 590, 1895–1906 (2012). [PubMed: 22351634]
42. Wakabayashi I, Poteser M, Groschner K, Intracellular pH as a determinant of vascular smooth muscle function. J. Vasc. Res 43, 238–250 (2006). [PubMed: 16449818]
43. Boedtkjer E, Aalkjaer C, Intracellular pH in the resistance vasculature: Regulation and functional implications. J. Vasc. Res 49, 479–496 (2012). [PubMed: 22907294]
44. Philipson KD, Bersohn MM, Nishimoto AY, Effects of pH on Na^+-Ca^{2+} exchange in canine cardiac sarcolemmal vesicles. Circ. Res 50, 287–293 (1982). [PubMed: 7055859]
45. Fabiato A, Fabiato F, Effects of pH on the myofilaments and the sarcoplasmic reticulum of skinned cells from cardiace and skeletal muscles. J. Physiol 276, 233–255 (1978). [PubMed: 25957]
46. Mandel F, Kranias EG, Grassi de Gende A, Sumida M, Schwartz A, The effect of pH on the transient-state kinetics of Ca^{2+}-Mg^{2+}-ATPase of cardiac sarcoplasmic reticulum. A comparison with skeletal sarcoplasmic reticulum. Circ. Res 50, 310–317 (1982). [PubMed: 6120049]
47. Komukai K, Pascarel C, Orchard CH, Compensatory role of CaMKII on ICa and SR function during acidosis in rat ventricular myocytes. Pflugers Arch. 442, 353–361 (2001). [PubMed: 11484765]
48. Touyz RM, Schiffrin EL, Effects of angiotensin II and endothelin-1 on platelet aggregation and cytosolic pH and free Ca^{2+} concentrations in essential hypertension. Hypertension 22, 853–862 (1993). [PubMed: 8244517]
49. Iino M, Kobayashi T, Endo M, Use of ryanodine for functional removal of the calcium store in smooth muscle cells of the guinea-pig. Biochem. Biophys. Res. Commun 152, 417–422 (1988). [PubMed: 3358768]
50. Nixon GF, Mignery GA, Somlyo AV, Immunogold localization of inositol 1,4,5-trisphosphate receptors and characterization of ultrastructural features of the sarcoplasmic reticulum in phasic and tonic smooth muscle. J. Muscle Res. Cell Motil 15, 682–700 (1994). [PubMed: 7706424]
51. Westcott EB, Goodwin EL, Segal SS, Jackson WF, Function and expression of ryanodine receptors and inositol 1,4,5-trisphosphate receptors in smooth muscle cells of murine feed arteries and arterioles. J. Physiol 590, 1849–1869 (2012). [PubMed: 22331418]
52. Hill-Eubanks DC, Werner ME, Heppner TJ, Nelson MT, Calcium signaling in smooth muscle. Cold Spring Harb. Perspect. Biol 3, a004549 (2011). [PubMed: 21709182]
53. Iino M, Kasai H, Yamazawa T, Visualization of neural control of intracellular Ca^{2+} concentration in single vascular smooth muscle cells in situ. EMBO J. 13, 5026–5031 (1994). [PubMed: 7957068]
54. Iino M, Endo M, Calcium-dependent immediate feedback control of inositol 1,4,5-triphosphate-induced Ca^{2+} release. Nature 360, 76–78 (1992). [PubMed: 1331809]
55. Lin P.-j., Luby-Phelps K, Stull JT, Properties of filament-bound myosin light chain kinase. J. Biol. Chem 274, 5987–5994 (1999). [PubMed: 10026225]
56. Denker SP, Huang DC, Orlowski J, Furthmayr H, Barber DL, Direct binding of the Na–H exchanger NHE1 to ERM proteins regulates the cortical cytoskeleton and cell shape independently of H^+ translocation. Mol. Cell 6, 1425–1436 (2000). [PubMed: 11163215]
57. Johnson RP, El-Yazbi AF, Takeya K, Walsh EJ, Walsh MP, Cole WC, Ca^{2+} sensitization via phosphorylation of myosin phosphatase targeting subunit at threonine-855 by Rho kinase

contributes to the arterial myogenic response. J. Physiol 587, 2537–2553 (2009). [PubMed: 19359365]

58. Tominaga T, Ishizaki T, Narumiya S, Barber DL, p160ROCK mediates RhoA activation of Na–H exchange. EMBO J. 17, 4712–4722 (1998). [PubMed: 9707430]
59. Baumgartner M, Patel H, Barber DL, Na^+/H^+ exchanger NHE1 as plasma membrane scaffold in the assembly of signaling complexes. Am. J. Physiol. Cell Physiol 287, C844–C850 (2004). [PubMed: 15355855]
60. Elf S, Blevins D, Jin L, Chung T-W, Williams IR, Lee BH, Lin J-X, Leonard WJ, Taunton J, Khoury HJ, Kang S, p90RSK2 is essential for FLT3-ITD– but dispensable for BCR–ABL-induced myeloid leukemia. Blood 117, 6885–6894 (2011). [PubMed: 21527514]
61. Billaud M, Lohman AW, Straub AC, Looft-Wilson R, Johnstone SR, Araj CA, Best AK, Chekeni FB, Ravichandran KS, Penuela S, Laird DW, Isakson BE, Pannexin1 regulates α1-adrenergic receptor– mediated vasoconstriction. Circ. Res 109, 80–85 (2011). [PubMed: 21546608]
62. Hong K, Cope EL, DeLalio LJ, Marziano C, Isakson BE, Sonkusare SK, TRPV4 (Transient Receptor Potential Vanilloid 4) Channel-dependent negative feedback mechanism regulates Gq protein-coupled receptor-induced vasoconstriction. Arterioscler Thromb. Vasc. Biol 38, 542–554 (2018). [PubMed: 29301784]
63. Sonkusare SK, Dalsgaard T, Bonev AD, Hill-Eubanks DC, Kotlikoff MI, Scott JD, Santana LF, Nelson MT, AKAP150-dependent cooperative TRPV4 channel gating is central to endothelium-dependent vasodilation and is disrupted in hypertension. Sci. Signal 7, ra66 (2014). [PubMed: 25005230]
64. Aalkjaer C, Cragoe EJ Jr., Intracellular pH regulation in resting and contracting segments of rat mesenteric resistance vessels. J. Physiol 402, 391–410 (1988). [PubMed: 2976824]
65. Thomas JA, Buchsbaum RN, Zimniak A, Racker E, Intracellular pH measurements in Ehrlich ascites tumor cells utilizing spectroscopic probes generated in situ. Biochemistry 18, 2210–2218 (1979). [PubMed: 36128]
66. Maravall M, Mainen ZF, Sabatini BL, Svoboda K, Estimating intracellular calcium concentrations and buffering without wavelength ratioing. Biophys. J 78, 2655–2667 (2000). [PubMed: 10777761]
67. Chu P-L, Gigliotti JC, Cechova S, Bodonyi-Kovacs G, Chan F, Ralph DL, Howell N, Kalantari K, Klibanov AL, Carey RM, McDonough AA, Le TH, Renal collectrin protects against salt-sensitive hypertension and is downregulated by angiotensin II. J. Am. Soc. Nephrol 28, 1826–1837 (2017). [PubMed: 28062568]
68. Vandsburger MH, French BA, Helm PA, Roy RJ, Kramer CM, Young AA, Epstein FH, Multi-parameter in vivo cardiac magnetic resonance imaging demonstrates normal perfusion reserve despite severely attenuated β-adrenergic functional response in neuronal nitric oxide synthase knockout mice. Eur. Heart J 28, 2792–2798 (2007). [PubMed: 17602202]
69. Utepbergenov D, Hennig PM, Derewenda U, Artamonov MV, Somlyo AV, Derewenda ZS, Bacterial expression, purification and in vitro phosphorylation of full-length ribosomal S6 kinase 2 (RSK2). PLOS ONE 11, e0164343 (2016). [PubMed: 27732676]

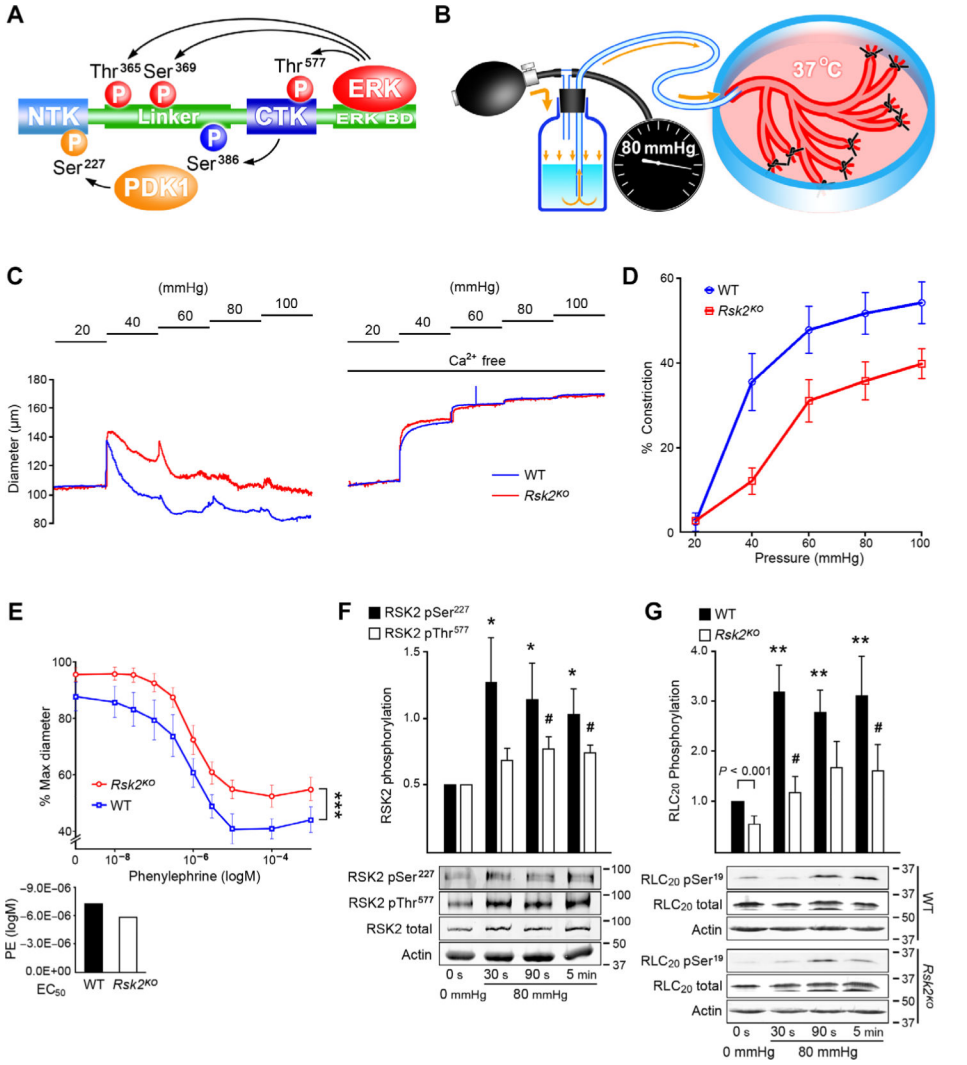

Fig. 1. Myogenic- and phenylephrine-induced vasoconstriction with associated RSK2 and RLC_{20} phosphorylation in WT and *Rsk2KO* mesenteric arteries measured by pressurization and Western blotting.

(**A**) Scheme showing the phosphorylation cascade for activation of RSK2. (**B**) Cartoon showing the apparatus for controlled luminal pressurization of mouse mesenteric artery cascades to obtain sufficient material for biochemical analysis of phosphorylation events. (**C**) Typical traces showing myogenic constriction of WT and $Rsk2^{KO}$ mesenteric arteries in response to increases in intraluminal pressure in Ca^{2+}-containing and Ca^{2+}-free Krebs solution. (**D**) Summary of myogenic responses of $Rsk2^{KO}$ and WT arteries at 40, 60, 80, and 100 mmHg. $P < 0.001$, $P < 0.01$, $P < 0.01$, and $P < 0.01$, respectively, determined by two-way analysis of variance (ANOVA). $Rsk2^{KO}$: $n = 3$ mice and 6 arteries; WT: $n = 3$ mice and 6 arteries. (**E**) Phenylephrine (PE) concentration responses of $Rsk2^{KO}$ and WT third- and fourth-order mesenteric arteries pressurized to 80 mmHg. ***$P = 0.005$ determined by two-way ANOVA. $Rsk2^{KO}$: $n = 3$ mice and 7 arteries; WT: $n = 3$ mice and 6 arteries. EC_{50} values for phenylephrine-induced contractions (bar graph) were not significantly different. P values were determined by two-tailed homoscedastic Student's t test. (**F**) Time course of

RSK2 phosphorylation (normalized to total RSK2) at the MEK/ERK Thr^{577} site and at the PDK Ser^{227} site following a pressure step from 20 to 80 mmHg in WT arteries. Data are means ± SEM; $n = 6$ mice and 6 arteries for each time point for Ser^{227} and 5 mice and 5 arteries for each time point for Thr^{577}. $^{*}P < 0.05$ for each time point compared to the corresponding control phosphorylation for Ser^{227}; $^{\#}P < 0.05$ for each time point compared to the corresponding control phosphorylation for Thr^{577}, two-tailed homoscedastic Student's *t* test. (**G**) Time course of RLC_{20} Ser^{19} phosphorylation following a pressure step from 20 to 80 mmHg in WT and $Rsk2^{KO}$ artery arcades. Data are means ± SEM; $n = 11$ WT mice and 11 arteries for each time point and $n = 4$ $Rsk2^{KO}$ mice and 4 arteries for each time point. $^{**}P < 0.01$ for each time point after an increase in pressure, compared to Ser^{19} phosphorylation in 0-mmHg pressure WT arteries; $^{\#}P < 0.05$ for each time point compared to Ser^{19} phosphorylation in 0-mmHg pressure $Rsk2^{KO}$ arteries, two-tailed homoscedastic Student's *t* test.

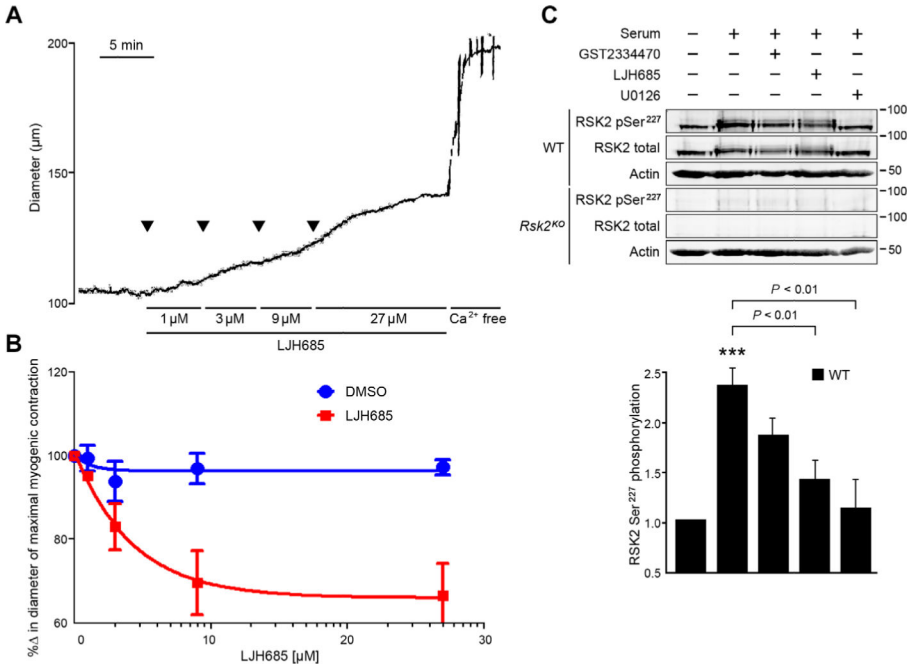

Fig. 2. The RSK inhibitor LJH685 induces relaxation of myogenic tone in mesenteric arteries and suppresses RSK2 phosphorylation in WT smooth muscle cells.

(**A** and **B**) Tension trace and summary showing relaxation of myogenic tone in response to increasing concentrations of LJH685 in a mesenteric artery in Krebs bicarbonate buffer and pressurized to 60 mmHg. Subsequent treatment with Ca^{2+}-free solution induced maximal vessel dilation. Dimethyl sulfoxide (DMSO) diluent concentrations were matched to LJH685 concentrations. $n = 3$ to 7 arteries per group. $P = 0.04$ for DMSO compared to LJH685 treatment, two-way ANOVA. (**C**) RSK2 Ser^{227} phosphorylation (normalized to total RSK2) in response to serum application in serum-starved mouse aortic smooth muscle cells or preincubation with LJH685, the PDK1 inhibitor GSK2334470, and the ERK1/2 inhibitor U0126. $Rsk2^{KO}$ smooth muscle cells served as a control. ***$P < 0.001$ control compared to serum stimulation, two-tailed homoscedastic Student's t test. Data are means ± SEM; $n = 3$ biological replicates per group.

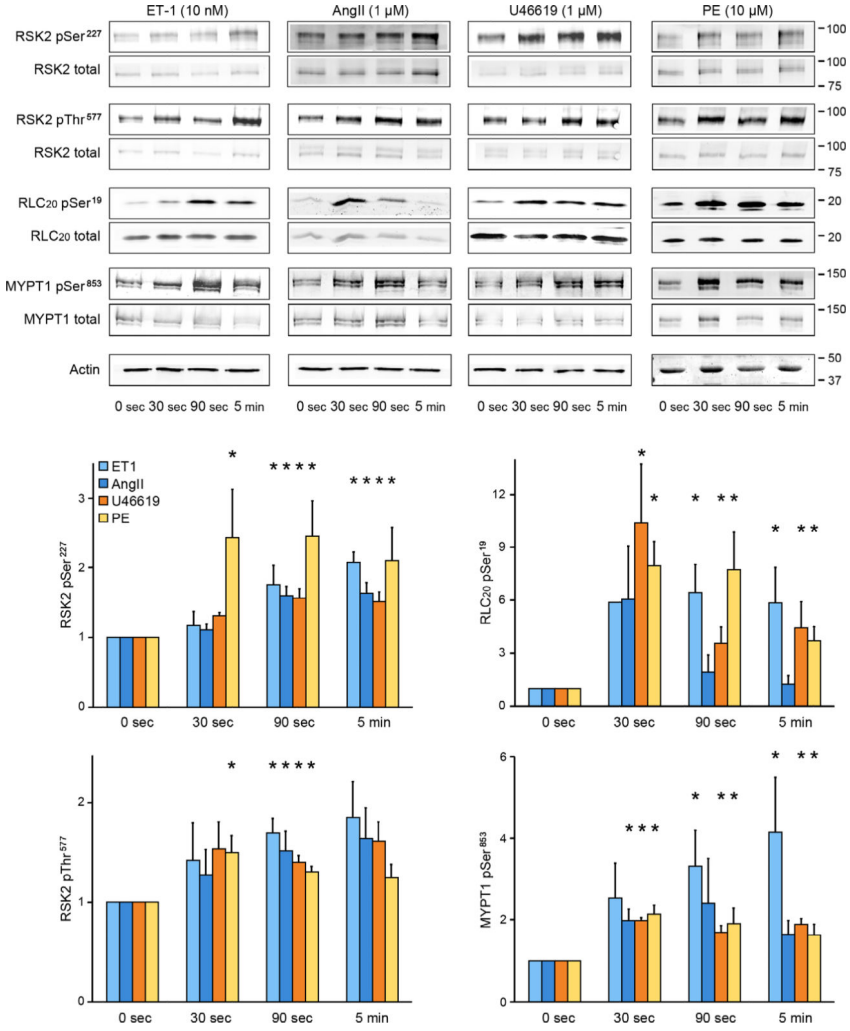

Fig. 3. Western blot analysis for agonist activation of RSK2, RLC_{20}, and MYPT1 phosphorylation in mouse mesenteric artery arcades.

Phosphorylation of Ser^{227} and Thr^{577} in RSK2 of Ser^{19} in RLC_{20} and Thr^{853} in MYPT1 (the ROCK site) under resting conditions compared to responses over time to ET-1, AngII, the thromboxane analog U46619, and phenylephrine. The doublets seen for RSK2 and MYPT1 in the Western blots (WB) likely reflect RSK2 isoforms (National Center for Biotechnology Information accession numbers NM 001346675.1 and NM 148925.2) and the two MYPT1 isoforms. Data are means ± SEM; $n = 3$ mice per agonist group and 3 artery samples per time point. $^*P < 0.05$ for each time point compared to the corresponding control (0 s) for each agonist. P values were determined by two-tailed homoscedastic Student's t test.

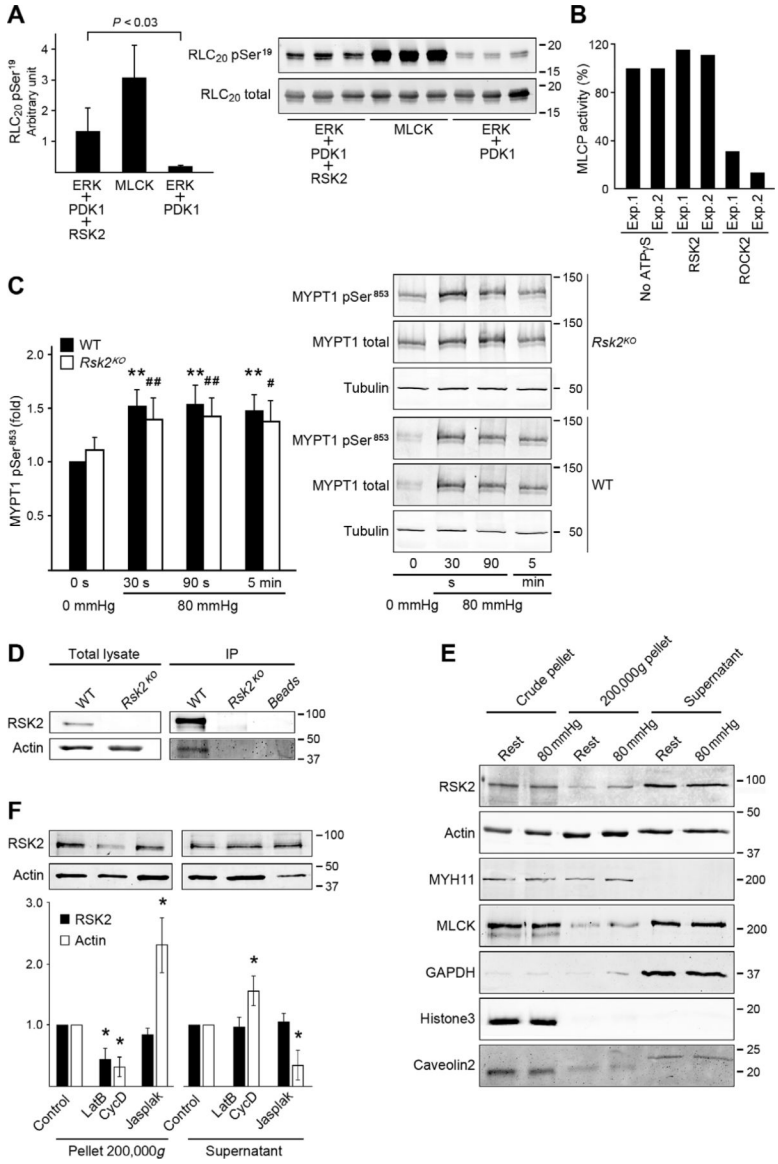

Fig. 4. RSK2 phosphorylation of RLC_{20}, effect on MLCP activity and immunoprecipitation, and fractionation assays to assess RSK2 association with actin.

(**A**) Phosphorylation of purified RLC_{20} protein at Ser^{19} by recombinant active RSK2. $n = 3$ independent experiments each carried out in triplicate, homoscedastic Student's t test. MLCK served as a positive control. (**B**) Effect of RSK2- or ROCK2-mediated phosphorylation of MYPT1 on in vitro MLCP activity. Bars show values of relative MLCP activity compared to the sample without adenosine 5′-(3-thio)triphosphate (ATPγS) thiophosphorylation. Two independent experiments each carried out in triplicate. (**C**) Phosphorylation of MYPT1 Thr^{853} (normalized to total MYPT1) over time in response to an increase in pressure from 0 to 80 mmHg in arteries from WT and *Rsk2*^{KO} mice. WT: $n = 8$ mice; *Rsk2*^{KO}: $n = 5$ mice. WT: $^{**}P < 0.01$; *Rsk2*^{KO}: $^{\#}P < 0.05$, $^{\#\#}P < 0.01$, two-tailed homoscedastic Student's t test. There was no significant difference between WT compared to *Rsk2*^{KO} at any time point. (**D**) Representative WB of RSK2 immunoprecipitation (IP) of actin from aortic smooth muscle cell lysates from WT and *Rsk2*^{KO} mice ($n = 3$ biological

replicates). (**E**) WB of fractions from lysates of mesenteric arteries at 0- or 80-mmHg pressure, showing RSK2 and MLCK in the 200,000*g* pellet. Myosin (MYH11) and glyceraldehyde-3-phosphate dehydrogenase (GAPDH) mark the cytoskeletal (200,000*g* pellet) and cytosolic fractions (supernatant), respectively; histone3 and caveolin2 mark the nuclear and membrane fractions and unbroken cells in the crude pellet ($n = 4$ mice and 4 artery arcades). (**F**) WB analysis of the effect of actin depolymerization by latrunculin B (LatB) plus cytochalasin D (CycD) or of actin polymerization by jasplakinolide (Jasplak) on the distribution of RSK2 and actin in the supernatant and high-speed spin pellets from mouse aortic smooth muscle cells. $^*P < 0.05$ compared to control, two-tailed homoscedastic Student's *t* test. $n = 4$ biological replicates. The concentrations of RSK2 in the supernatant were not significantly changed by treatment.

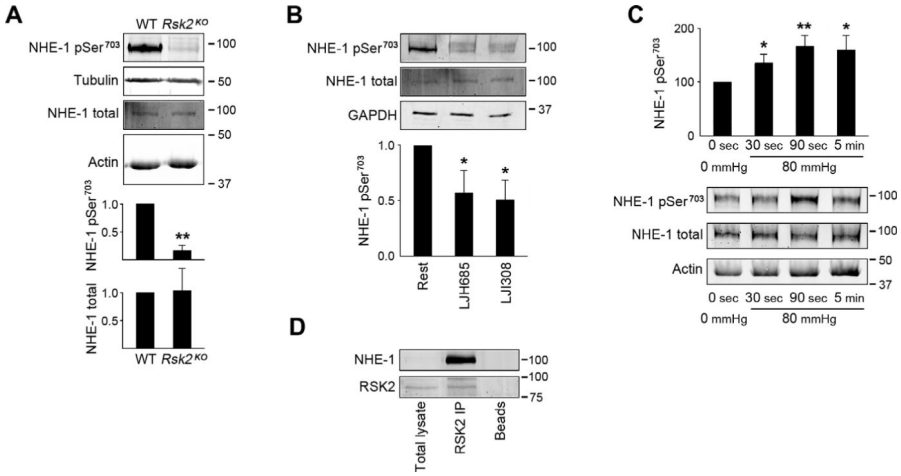

Fig. 5. RSK2 regulation of Na^+/H^+ exchanger activity as assessed by phosphorylation and immunoprecipitation measurements.

(**A**) WB showing phosphorylation of NHE-1 Ser^{703} (normalized to total NHE-1) in WT and *Rsk2*^{KO} mesenteric arteries. Data are means ± SEM; $n = 3$ mice per group; $^{**}P < 0.01$. (**B**) WB showing phosphorylation of NHE-1 Ser^{703} (normalized to total NHE-1) in untreated WT mesenteric arteries or those treated with the RSK inhibitor LJH685 or LJI308. Data are means ± SEM; $n = 3$ mice per group. $^{*}P < 0.05$ for LJH685 and LJI308 compared to untreated arteries. The doublet for phospho–NHE-1 likely reflects NHE-1 isoforms that are frequently detected by the more reactive phospho–NHE-1 antibody than the less reactive total NHE-1 antibody and under the conditions used for electrophoresis. (**C**) Time course of NHE-1 Ser^{703} phosphorylation normalized to total NHE-1 in response to increased arterial intraluminal pressure. Data are means ± SEM; $n = 6$ mice and 6 artery samples per time point. $^{*}P < 0.05$, $^{**}P < 0.01$, time points compared to 0 s, two-tailed homoscedastic Student's *t* test. (**D**) Representative WB assay showing NHE-1 immunoprecipitation from mesenteric artery homogenates by RSK2 antibody ($n = 4$ mesenteric arcades from four mice analyzed separately). The lack of an NHE-1 band in the total lysate is due to the low intensity used to scan the membrane to not saturate the NHE-1–immunoprecipitated band.

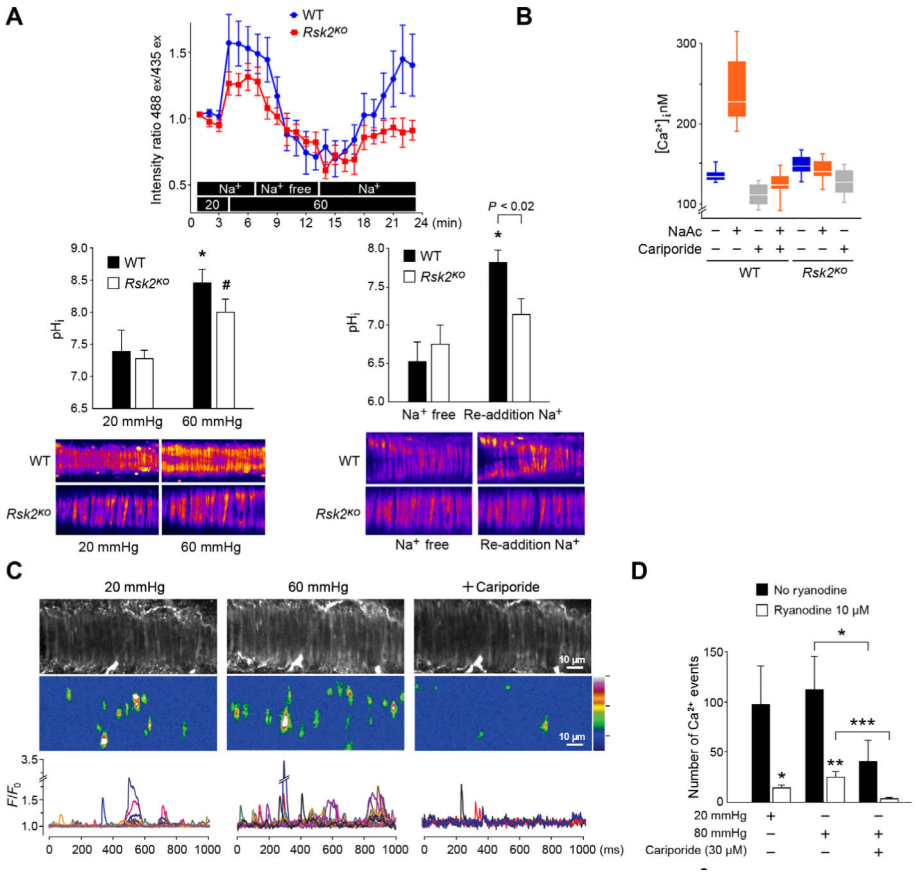

Fig. 6. RSK2 activation of the Na^+/H^+ exchanger increases intracellular pH and Ca^{2+}.

(**A**) RSK2-regulated NHE-1 activity was monitored with the ratiometric fluorescent pH indicator BCECF-AM loaded into WT and *Rsk2*^{KO} mesenteric arteries. Bar graphs show conversion of intensity ratios to pH with typical fluorescent images of arteries. $n = 3$ mice per genotype and 6 arteries. $^*P < 0.05$, for 20-mmHg pressure compared to 60-mmHg pressure and for Na^+-free compared to re-addition of Na^+ for WT arteries; $^{\#}P < 0.02$, for 20 mmHg compared to 60 mmHg in *Rsk2*^{KO} arteries, two-tailed homoscedastic Student's *t* test. The last three pH values for WT and *Rsk2*^{KO} arteries upon re-addition of Na^+ are averaged in the bar graph. (**B**) Cytosolic Ca^{2+} measured in WT and *Rsk2*^{KO} aortic smooth muscle cells treated with sodium acetate (NaAc) to stimulate NHE-1, with or without the NHE-1 inhibitor cariporide. $n = 3$ biological replicates per genotype. $P < 0.0002$ for $[Ca^{2+}]$ in WT cells before and after treatment with NaAc, two-tailed homoscedastic Student's *t* test. (**C**) Typical example of Ca^{2+} transient analysis in WT mesenteric arteries in the presence of 10 µM ryanodine to block Ca^{2+} release from the ryanodine-sensitive Ca^{2+} stores. Gray-scale images showing smooth muscle cells in an artery. Typical Ca^{2+} fluorescent intensity images of all the event sites in the field summed over 1000 ms. F/F_0 traces of cytoplasmic Ca^{2+} transients. Each color represents a trace from a region in a different cell. (**D**) Summary of Ca^{2+} events at 20- and 60-mmHg intraluminal pressure in the presence and absence of cariporide and/or ryanodine. Data are means ± SEM. $^*P < 0.05$, $^{***}P < 0.001$, $n = 4$ mice and 6 arteries without ryanodine. $^*P < 0.05$, $^{**}P < 0.01$, $n = 4$ mice and 6 arteries with ryanodine treatment.

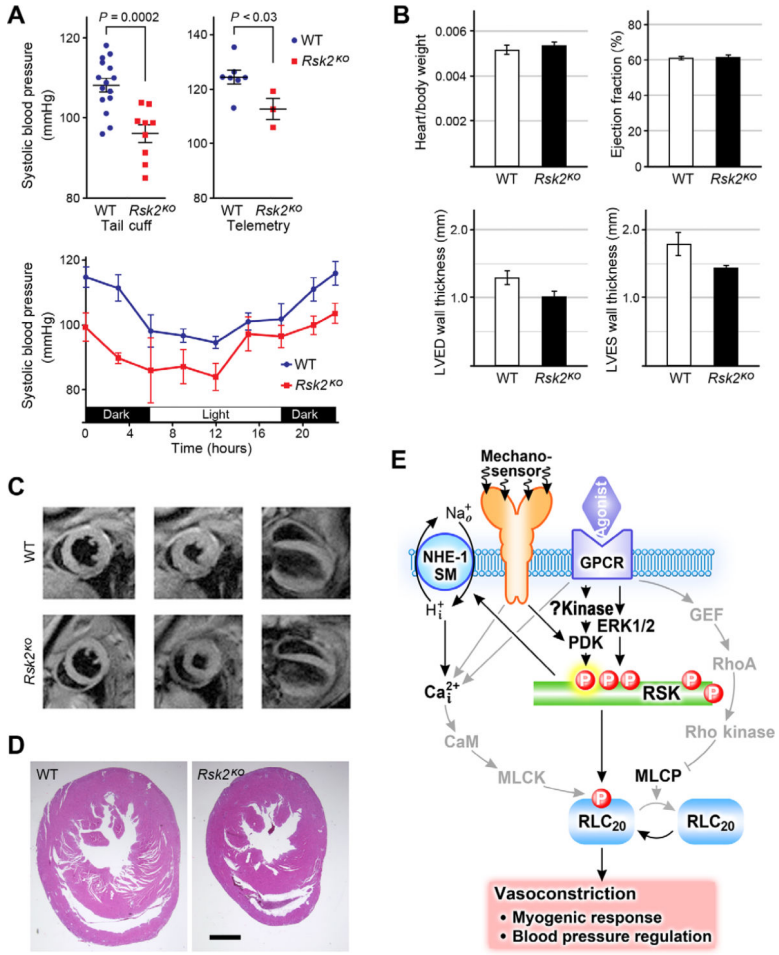

Fig. 7. Blood pressure and cardiac function measurements in *Rsk2*^{KO} mice.

(**A**) Tail cuff measurements in male and female WT and *Rsk2*^{KO} mice. $n = 9$ *Rsk2*^{KO} mice, $n = 15$ WT mice. Systolic blood pressure mean ± SEM. $P < 0.003$ for female *Rsk2*^{KO} mice compared to WT female mice; $P < 0.001$ for male *Rsk2*^{KO} mice compared to WT male mice, two-tailed homoscedastic Student's *t* test. Radiotelemetric measurements of blood pressure in WT and *Rsk2*^{KO} blood pressure over 24 hours. $n = 7$ WT males, $n = 3$ *Rsk2*^{KO} males. Data are means ± SEM for systolic blood pressures. (**B**) Heart/body weights; $n = 8$ WT and 9 *Rsk2*^{KO} mice. Male and female mice were averaged together because there was no statistically significant difference in the ratios. MRI analysis, $n = 3$ mice per group. (**C**) Typical MR images used to calculate cardiac wall thickness and ejection fraction. Left column, diastole; middle column, systole; right column, longitudinal view, diastole. (**D**) Histological cardiac sections of WT and *Rsk2*^{KO} mice. $n = 3$ mice per group. (**E**) Scheme showing RSK2 signaling in smooth muscle and its contribution to vasoconstriction, the myogenic response, and blood pressure regulation. GPCRs and pressure-sensitive mechanosensors activate RSK2 through activation of ERK1/2 or another, as yet unidentified kinase to activate PDK. Active RSK2 phosphorylates and activates two targets, RLC_{20} and NHE-1, leading to alkalinization of the cell and increased $[Ca^{2+}]_i$, which, in turn, augments MLCK activity and promotes vasoconstriction.